



HORIZON EUROPE PROGRAMME – TOPIC: HORIZON-CL5-2022-D5-01-02

## AENEAS

### innovActive ENERgy storage systems onboArd vessels

#### Deliverable 5.1: HIL simulation models for ship power system

<b>Primary Author(s)</b>	Tariq Kamal, Reza Naghash   UVA
<b>Deliverable Type</b>	Report
<b>Dissemination Level</b>	Sensitive
<b>Due Date (Annex I)</b>	31.03.2025 (Month 26)
<b>Pages</b>	63
<b>Document Version</b>	Final
<b>GA Number</b>	101095902
<b>Project Coordinator</b>	Mohsen Akbarzadeh   Flanders Make (FM) (Mohsen.Akbarzadeh@flandersmake.be)

Contributors	
Name	Organisation
Tariq Kamal	UVA
Reza Naghash	UVA
Kimmo Kauhaniemi	UVA

Formal Reviewers	
Name	Organisation
Anesa Begovic	I2M
Franck Sellier	SIE

Version Log			
Rev #	Date	Author	Description
0.1	28.02.2025	Tariq Kamal (UVA)	Draft
0.2	12.03.2025	Reza Naghash (UVA)	Contributions
0.3	18.03.2025	Kimmo Kauhaniemi (UVA)	Editing and reviewing
0.4	19.03.2025	Tariq Kamal (UVA)	Final revision
<b>1.0</b>	26.03.2025	Anesa Begovic (I2M)	Quality review
<b>2.0</b>	28.03.2025	Franck Sellier (SIE)	Quality review
<b>3.0</b>	23.04.2025	Mohsen Akbarzadeh (FM)	Coordinator review and approval, deliverable ready for submission

## Project Abstract

AENEAS aims to contribute towards climate-neutral and environmentally friendly water transport through three new next generation clean energy storage solutions. Eventual impact is an increase of the global competitiveness of the EU waterborne transport sector by European technology leadership for energy storage solutions for diverse waterborne applications.

AENEAS will develop three innovative electric Energy Storage Solutions (ESS) for waterborne transport, which are advanced beyond the traditional battery systems, including Solid-state batteries (SSB), Supercapacitors (SC) and a Hybrid system which combines SSB and SC.

The solutions enable (partial or full) electric shipping, considering conditions specific ships might encounter, including adverse conditions outside sheltered waters or going upstream on rivers. AENEAS will evaluate them for a range of applications and end uses in short-sea shipping and in-land waterways. At the same time AENEAS will define the pathway for the three ESSs for application in different ship types, achieving a comprehensive understanding of the ESSs and their applicability for diverse waterborne transport.



## Table of Contents

Public Summary .....	5
1 Introduction .....	6
1.1 Rational of this deliverable .....	6
1.2 Overview of contributors and contributions .....	6
1.3 Alignment with WP1–WP4 and future deliverables .....	7
1.4 Structure of the document.....	7
2 Objectives and scope of HIL model development .....	9
2.1 Real-time simulation goals and requirements .....	9
2.2 Integration with previous work packages.....	9
2.3 Model development strategy for HIL testing .....	9
3 Development of HIL simulation models.....	11
3.1 Use case 1: SSB.....	11
3.1.1 Power system design.....	11
3.1.2 Power Management System .....	14
3.1.3 Control system design .....	16
3.1.4 SSB in HIL platform .....	22
3.2 Use case 2: SC.....	24
3.2.1 Power system design.....	24
3.2.2 Power Management System .....	27
3.2.3 Control system design .....	28
3.2.4 SC in HIL platform .....	33
3.3 Use case 3: Hybrid ESS (SSB and SC) .....	34
3.3.1 Power system design.....	34
3.3.2 Power Management System .....	35
3.3.3 Control system design .....	36
4 Real-time Simulation Setup .....	39
5 HIL simulation results .....	41



5.1 Use case 1.....	41
5.2 Use case 2.....	45
5.3 Use case 3.....	49
6 Conclusions and future work .....	52
6.1 Summary of D5.1.....	52
6.2 Plans for transition to next task .....	52
6.3 Conclusions .....	53
7 References.....	54
8 Abbreviation list .....	55
9 Acknowledgements and disclaimer.....	56
List of Figures.....	57
Annex 1: General arrangement and technical specification of Ro-ro ships.....	60
Annex 2: General arrangement and technical specification of Cruise – series ship.....	62



## Public Summary

This document is a part of Task 5.1 in WP5, where the aim was to develop simulation models of ship power system, ESS, power converters, and control system. This deliverable provides the real-time Hardware-in-the-Loop (HIL) simulation models specifically designed for validating innovative Energy Storage Solutions (ESS) onboard maritime vessels within the AENEAS project. These ESS technologies include Solid-State Batteries (SSB), Supercapacitors (SC), and Hybrid ESS (integrating SSB and SC). The developed HIL simulation models encompass comprehensive ship power system components, including diesel generators, energy storage systems, and loads, as well as critical power electronics components such as bidirectional DC-DC converters and inverters with their low-level control system. As this task is a fundamental part for experimental testing of the ESS with their power electronics converters, this work mainly focused on detailed design on power electronics and control systems, to ensure the stability and dynamic response of the ESS and power electronics system in the case of connection to a shipboard microgrid. These models integrate realistic operational profiles, electro-thermal characterization, optimization strategies, and component models previously developed and validated in previous work packages WP1-WP4. Utilizing MATLAB, PSIM and Typhoon HIL platforms, the simulation models provide a realistic framework for thoroughly testing and validating ESS technologies, and power management strategies in real-time. This deliverable significantly advances the understanding and application of ESS technologies, ensuring enhanced efficiency, safety, reliability, and sustainability in maritime transportation.

# 1 Introduction

## 1.1 Rational of this deliverable

This deliverable, “HIL simulation models for ship power system” is a part of Task 5.1 in WP5. Simulation models of ship power system, ESS, and power converters addresses a critical step in the AENEAS project's roadmap, focusing on developing robust real-time HIL simulation models for validating innovative ESS and power/energy management systems onboard maritime vessels. The development of these sophisticated simulation models is essential due to the inherent complexities and rigorous operational demands encountered in maritime environments, including variable power demands, dynamic load scenarios, and strict safety requirements.

On other hand, as this project is going to test the innovative ESS prototypes in real use cases similar to the shipboard power systems through power electronics converters, designing the power converter and control system is a crucial step. Therefore, this deliverable focuses on designing power stage and control stage of the power electronics systems especially storage side converters considering real-time switching behaviour, to achieve desired dynamic response of proposed solutions.

The maritime sector is actively seeking climate-neutral and environmentally friendly transportation solutions, thereby increasing the need for accurate simulation-based validation methods that ensure the reliability and efficiency of newly introduced technologies. The AENEAS project specifically targets next-generation ESS, including SSB, SC, and hybrid combinations, which require thorough validation under realistic operational scenarios to meet required performance, safety, and longevity.

Real-time HIL simulations developed in this deliverable provide a cost-effective, safe, and flexible validation environment to thoroughly test ESS and energy management strategies before actual deployment onboard ships. Utilizing advanced simulation tools like PSIM and Typhoon HIL, these models incorporate extensive data from electro-thermal characterizations, optimized control strategies, and realistic load profiles developed in previous work packages.

The developed real-time HIL platform in this deliverable is the fundamental step to achieve the Power Hardware-in-the-Loop (PHIL) testbed for the next tasks in WP5. This PHIL setup integrates bidirectional DC sources (to emulate SSB and SC) and/or real SSB and SC modules, DC-DC converters, inverters, and a three-phase programmable power supply and load that is emulating the rest of the shipboard microgrid. This advanced PHIL framework ensures accurate representation of shipboard power systems by enabling real-time simulation under dynamic maritime operational conditions. The development and validation efforts undertaken in D5.1 significantly strengthen technological advancements in maritime energy storage and power electronics, directly aligning with AENEAS's objectives for cleaner, sustainable, and competitive waterborne transport.

## 1.2 Overview of contributors and contributions

UVA coordinated the development of real-time simulation models, contributing their expertise in power electronics, control, and HIL technology. UVA developed the core HIL simulation platform, covering models of ESS, generators, power converters, control system, PMS, and ancillary loads. SIE provided essential pre-design models for key power system components and energy storage, enhancing realism in simulations. Their contributions enabled accurate emulation of real system behaviors and supported model validation against experimental data.

ABEE and CEA offered electro-thermal characterization data for ESS, providing validated parameters that ensure precise ESS behavior simulation under maritime conditions.

AUTH contributed significantly with advanced thermal analyses for validating thermal management strategies under realistic conditions and ensuring ESS thermal stability and safety during maritime operation. FM contributed by developing optimization strategies, conceptual ESS module designs, and thermal management solutions.

### 1.3 Alignment with WP1–WP4 and future deliverables

This deliverable integrates critical developments from earlier work packages. WP1 [1] provided detailed operational vessel profiles and scenarios that support realistic system modeling. WP2 [2] contributed to component-specific modeling and simulation strategies, which are essential for accuracy in real-time simulations. WP3 [3] delivered validated electro-thermal ESS models crucial for realistic ESS simulation. WP4 [4], contributed to detailed ESS module sizing, design requirements, thermal management, and safety criteria that were essential for accurate modeling.

The deliverable experienced a two-month delay primarily due to the unavailability of essential technical data and information from T2.3, which detailed technical specifications for ship power system optimization including the power converters sizing, PMS, and EMS required for accurate real-time modeling. Future deliverables include:

- D5.2: A downscaled real-time PHIL setup, led by UVA, focusing on adapting these detailed real-time simulations for practical hardware validation.
- D5.3: Downscaled hardware testing, validation, and demonstration of ESS solutions at TRL 5, led by UVA, applying real-time validated simulations in PHIL testing.
- D5.4: Up-scaled evaluation and validation of ESS solutions at the entire ship power and energy level, led by CEA, ensuring the validated technologies scale effectively from downscaled experiments to real-world maritime operations.

### 1.4 Structure of the document

This document is structured as:

- Section 1 provides an introduction including the rationale, an overview of the contributions from various partners, and alignment of this deliverable with previous and future deliverables.
- Section 2 specifies the objectives and scope, detailing the real-time simulation goals and requirements, integration methodologies with earlier work packages, and the overall strategy for model development.
- Section 3 extensively covers the development of HIL simulation models, structured into three use cases. Each use case is systematically detailed with modeling techniques, data requirements, specific power system designs, control system methodologies, ESS-specific modeling, and power management algorithms.
- Section 4 provides real-time setup that is developed to perform real-time simulation for introduced use cases.
- Section 5 presents the results obtained from HIL simulations for each use case, providing validation and analysis of performance under operational conditions.

- Section 6 concludes a summary of model developments and outlines future activities, including plan for transitioning towards downscaled hardware testing.
- Section 7 provides a list of references, followed by abbreviations list and acknowledgements in sections 8, and 9.

## 2 Objectives and scope of HIL model development

### 2.1 Real-time simulation goals and requirements

The primary goal of creating real-time simulation models within this deliverable is to provide a robust and realistic validation platform for testing advanced ship power system components, specifically innovative ESS, i.e., SSB, SC, and hybrid ESS configurations. These real-time simulations are designed to accurately replicate the dynamic operational conditions typically encountered in maritime environments, including transient responses during vessel manoeuvring, fluctuating load scenarios, and interaction of power electronics-based ESS blocks with conventional generation units such as diesel generators and shaft generators.

Specific objectives include:

- Ensuring accurate replication of vessel power system behaviours under realistic and operational scenarios.
- Validating the electrical performance, and reliability of ESS technologies.
- Assessing the effectiveness of advanced control algorithms and power management strategies in maintaining system stability, and efficiency.
- Providing a versatile and flexible testing environment to evaluate complex interactions among power system components, including EES, power converters, diesel generators, and ancillary loads.

### 2.2 Integration with previous work packages

HIL models developed in WP5 dependent on the outcomes and methods developed in previous WPs. WP1 provided essential operational vessel profiles and realistic scenarios that serve as references for WP5 simulations. These profiles provide information that WP5 models accurately represent real maritime operations. WP2 developed detailed component models and simulation strategies necessary for real-time simulations. Specifically, it created vessel simulation models for the Eco-Livorno Ro-Ro vessel, Roma cruise vessel, and Anaconda inland vessel using the Simcenter Amesim platform. These models, which represent energy exchanges between subsystems (powertrains, generators, loads, and energy storage systems), have been validated using WP1's mission profiles and subsequently integrated into WP5 simulations.

WP3 provided validated electro-thermal ESS models, capturing electrical and thermal characteristics such as internal resistance, thermal conductivity, heat capacity, and State of Charge (SoC) dynamics. WP4 contributed detailed ESS module designs, including sizing, thermal management, and safety requirements. WP5 considered all of these validated models in real-time simulations.

### 2.3 Model development strategy for HIL testing

The model development strategy used in HIL platform involved a structured approach using methodologies and simulation tools:

- Power and control stage design: Prior to the development of HIL simulation, the power electronics system including power converters, filters, control strategy, and controller coefficients are designed. Since there was no power electronics design in previous WPs and due to the lack of technical information about power electronics systems in real use cases, the design is proposed for the first time in the deliverables.

- Initial component modelling: First, detailed electrical and thermal component models were developed and validated using the MATLAB/SIMULINK and PSIM software environment, and next, developed in Typhoon HIL for real-time execution. These models captured accurate component dynamics, such as ESS charge-discharge characteristics, power electronics (converters/inverters) behaviour, generator performance, and load profiles. The real-time model results in Typhoon HIL matched with PSIM results.
- Real-time integration: Validated component models were subsequently integrated into the Typhoon HIL platform. In this stage, the MATLAB/SIMULINK and PSIM-derived models (especially the power stage and ESS, and controllers' dynamics) are imported or re-implemented on Typhoon HIL's real-time simulator. The Typhoon HIL environment runs the models in a few microseconds time steps (1 to 5  $\mu$ s depends on model the complexity), allowing it to emulate the system behaviour in real time. This real-time model is interfaced with actual hardware control units (microcontrollers), so that measured signals from Typhoon HIL device (voltages, currents, sensor readings) and control outputs from microcontrollers can be exchanged just as they would be in a physical system. This leads to a high-reliability real-time simulation that can interact with hardware, also called Controller Hardware-in-the-loop (CHIL).
- Control and power management algorithms: Control strategies are implemented to achieve stability and desired dynamic response considering shipboard microgrid constraints. A hierarchical PMS were incorporated directly into the real-time simulations to check SoC, power generation, and load balancing. These algorithms were optimized using data from previous WPs to ensure they meet maritime operational and performance criteria. For example, prior WPs have gathered load profiles or component characteristics that provide setpoints for the low-level control system.
- Testing and validation: Once integrated, the entire simulation environment tested testing, including validation against previously characterized experimental data (electrical and thermal) from previous WPs. This iterative validation process ensures model accuracy, and reliability in replicating real-world behaviours.
- Flexibility and scalability: The developed HIL simulation platform was designed with flexibility and scalability in mind, ensuring adaptability for future downscaled hardware tests and upscaled full-system demonstration. For example, one can replace certain simulated components with actual hardware (for a PHIL test of a new device) or conversely simulate the entire system for a large-scale scenario, without changing the overall framework. This flexibility means that it is easy to include new components or control strategies, and it can scale up to emulate the full integrated system in real-time. It can accommodate expansions or different configurations (e.g., adding more SSB, SC, motors, or generators).

This structured model development strategy as illustrated in Figure 1 ensures that the final HIL platform accurately meets the comprehensive simulation needs and stringent validation requirements set forth by the AENEAS project, providing significant insights into the performance and reliability of next-generation maritime energy storage solutions.

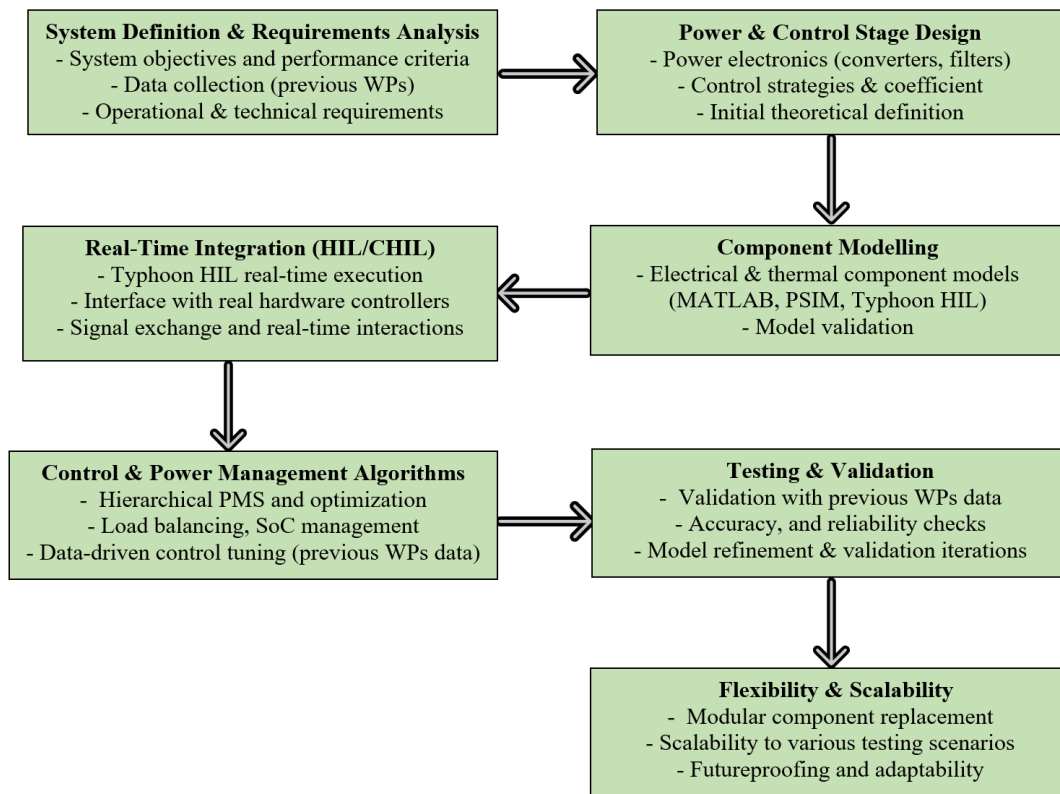


Figure 1: Block diagram of HIL model development strategy

## 3 Development of HIL simulation models

### 3.1 Use case 1: SSB

#### 3.1.1 Power system design

Based on the original architecture proposed in previous WPs, the shipboard microgrid architecture and corresponding power converters and filters are designed. The overall architecture of the shipboard for UC #1 (SSB) is depicted in Figure 2. The SSB packs are connected to the main DC bus through bidirectional DC-DC converters, and the DC-link is connected to the main AC bus by DC-AC converters and transformers. Diesel generators are feeding the main AC bus, based on the PMS/EMS command. The main AC bus voltage is 690V, and the output of the inverters are 600V, according to the original design of the shipboard power system. In the DC side, the SSB output voltage are in the range of 900V to 1.05kV (based on the corresponding SoC), which is converted to 1.2kV via Boost converters. The DC side is re-designed based on the innovative SSB modules. The shaft generators are also connected to the DC bus utilizing Active Front End (AFE) rectifiers.

Next, according to the load profile and required power and energy, the power rating of the shipboard microgrid components is determined. As this project focuses on storage side solutions, it focuses on DC-DC storage side and DC-AC interlink power converters. Based on the optimization in WP2, the power rating for each DC-DC power converter is 188kW to deliver the required energy from SSB to the load in the desired period. For this purpose, a bidirectional DC-DC converter is selected which is shown in Figure 3.

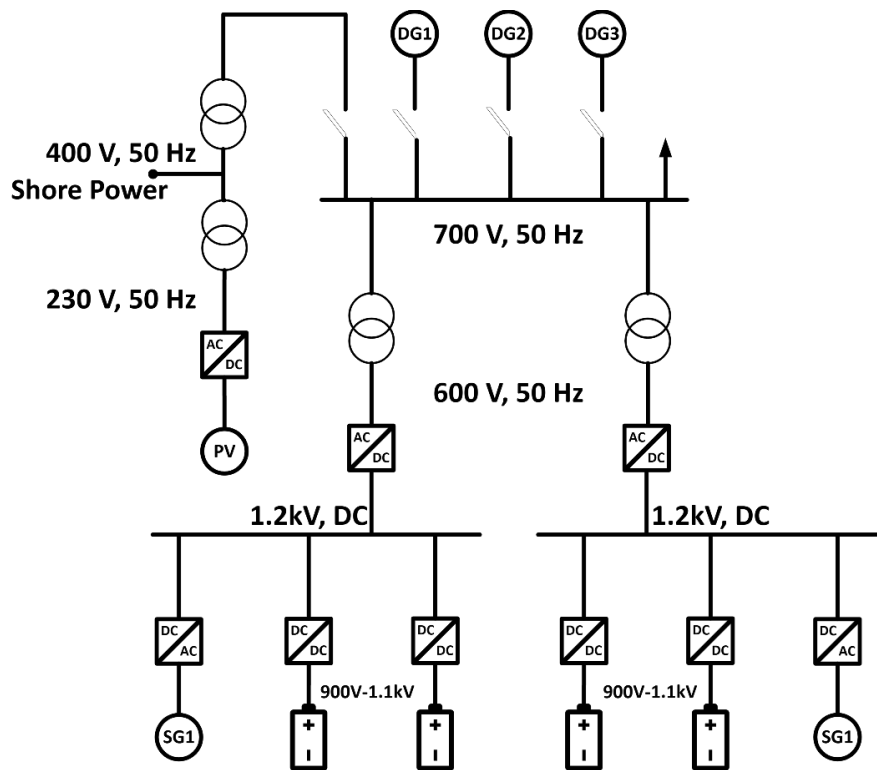


Figure 2: Shipboard microgrid for UC#1 (SSB)

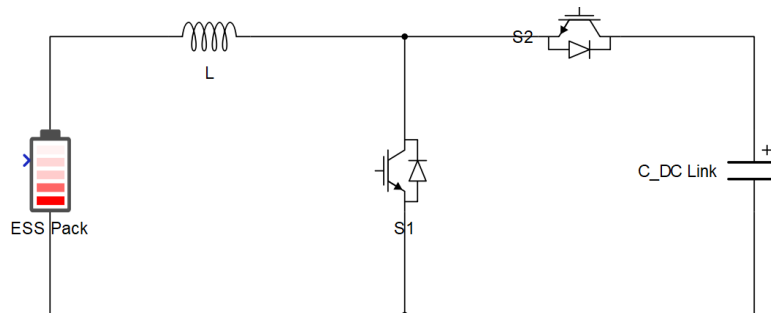


Figure 3: Bidirectional DC-DC converter

The input parameters to design the DC-DC converter are provided in Table 1.

Table 1: DC-DC converter specifications for UC#1

Parameter	Value
SSB minimum output voltage (V)	925
SSB nominal output voltage (V)	1050
DC-link Voltage (V)	1200
Output power (kW)	188
Inductor current ripple (%)	6
Maximum voltage ripple (%)	5
Switching frequency (kHz)	10

By calculating the maximum inductor current ( $I_{L,max}$ ) and output current ( $I_o$ ) by

$$I_{L,max} = \frac{P_o}{V_{SSB,min}} \quad (1)$$

$$I_o = \frac{P_o}{V_{dc}} \quad (2)$$

In which,  $P_o$ ,  $V_{SSB,min}$ ,  $V_{dc}$ , are the output power, minimum voltage of SSB, and DC-link voltage, respectively. Hence, the inductance and capacitance values can be determined:

$$L = \frac{V_{dc} \cdot D}{\Delta I_L \cdot f_{sw}} = 1.5 \text{ mH} \quad (3)$$

$$C = \frac{D \cdot I_o}{V_{ripple} \cdot f_{sw} \cdot V_{dc}} = 39.167 \text{ } \mu\text{F} \quad (4)$$

where  $\Delta I_L$ ,  $V_{ripple}$ ,  $D$ , are inductor maximum current ripple, DC-link maximum voltage ripple, and duty cycle of the power converter, respectively.

Next step is to design the three-phase interlink inverter/rectifier that is connected between the DC link and the main AC bus (through transformer). This converter utilizes an LCL filter in the output, to filter out the harmonics and ensure the controllability of the converter. The input parameters to design the LCL filter is provided in Table 2.

**Table 2: DC-AC converter specifications for UC#1**

Parameters	Value
AC bus frequency (Hz)	50
RMS line-line voltage (V)	600
Input DC voltage (V)	1200
Output power (kW)	2000
Maximum output current THD (%)	5
Minimum power factor	0.995
Switching frequency (kHz)	4
Resonance frequency (kHz)	0.8

The LCL filter is designed to attenuate the harmonics and achieve desire current ripple reduction while limiting the AC voltage drop and maintaining high power factor.

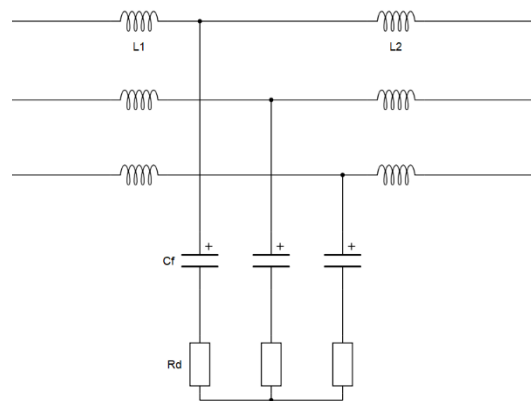


**Figure 4: LCL filter with passive damping resistance**

To ensure stability, the resonance frequency is set to one-fifth of the switching frequency, and the passive damping method is used in this case. This design is a reciprocal process, so the initial values are re-calculated in a few iterations to reach the proper values within the constraints. The three-phase LCL filter is provided in Figure 4, in which the  $L_1$  is converter side inductor,  $L_2$  is the grid side inductor,  $C_f$  is filter capacitor, and  $R_d$  is damping resistor.

The calculated values for the LCL filter are as follows:

$$\begin{aligned} L_1 &= 25.321 \mu H \\ L_2 &= 25.321 \mu H \\ C_f &= 3.8 mH \\ R_{d,min} &= 0.0084 \Omega \end{aligned}$$

As the damping resistor is crucial in the control system stability, the final value for the damping resistor is calculated in the process of controller design in the next section.

According to the inverter power level, the DC link capacitor should be larger than 5mF, to handle the maximum power and consider low-frequency ripples.

### 3.1.2 Power Management System

The operational scenarios are an essential part for design the control system for the HIL platform. According to the power generation units that is depicted in Figure 5, different operational cases can be determined.

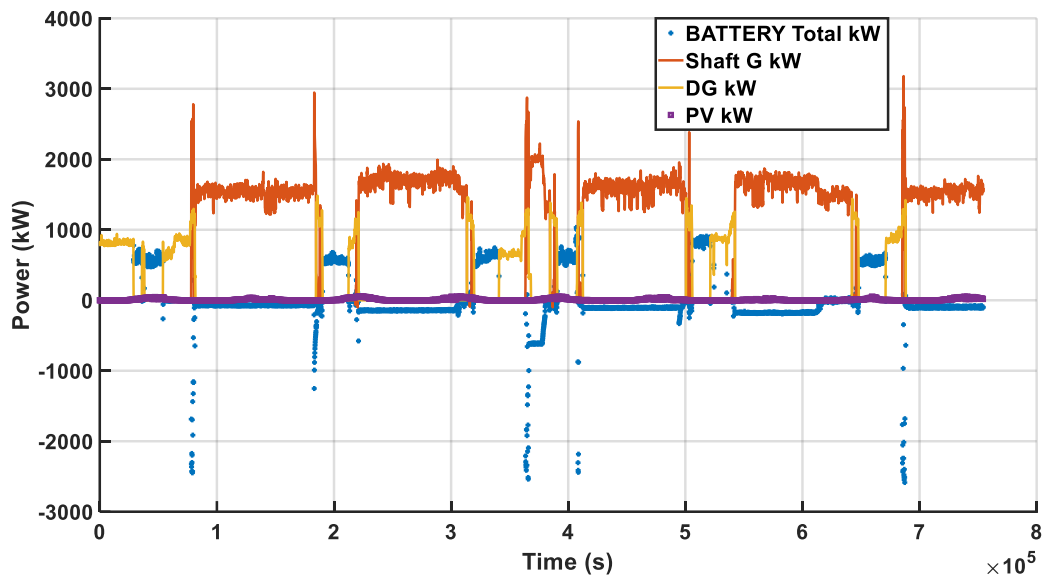


**Figure 5: Power generation units for UC#1**

First, by focusing on periods where the battery is discharging, the following conditions are observed:

- Battery is the only generation source; the DC-DC converter controls the output voltage (DC link) and its current, and the inverter is in grid-forming mode, in which controls output voltage and current.
- Battery is discharging alongside the diesel generators; the DC-DC converter is controlling the discharging current, and the inverter is controlling the DC link voltage and output current.
- Battery is discharging with both diesel generators and shaft generators; the DC-DC converter is controlling the discharging current, and the inverter is controlling the output current. Shaft generator is responsible for regulate DC link voltage by AFE rectifier.

Next, considering periods where the battery is charging, the DC-DC converter is controlling charge current or voltage (based on the BMS command), and the inverter or AFE rectifier injects required charge current to the batteries.

The power management system is controlling the power converters and setting the references to ensure the power sharing is done properly. The overall state chart of different cases is provided in Figure 6.

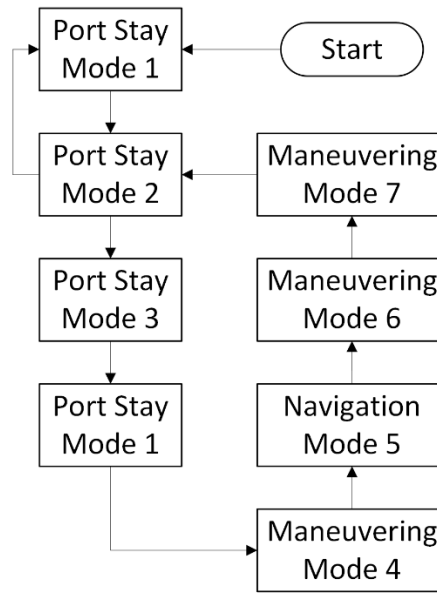


**Figure 6: Power management algorithm based on load profile for UC#1**

The definition for each mode is as follows:

- Mode 1: DG + PV (sometimes)
- Mode 2: Battery (discharging) + PV (sometimes)
- Mode 3: Battery (discharging) + DG + PV (sometimes)
- Mode 4: DG + SG + Battery (charging)
- Mode 5: SG + Battery (charging in CC mode)
- Mode 6: SG + DG + Battery (charging in CC/CV)
- Mode 7: SG +DG + Battery (discharging)

One of the main tasks of the PMS is to provide proper current (power) sharing among power generation sources through power converters control system. As this deliverable focuses on the battery operation, the current sharing among battery sources is considered in corresponding modes. A droop control strategy considering SoC of batteries is designed based on [9]. In this method, droop coefficients are selected by using (5), where  $R_{d,i,discharge}$  is droop coefficient of module,  $C_{BAT,i}$  is the corresponding module capacity, and  $C_{max}$  is the capacity of the battery with highest nominal capacity in the system. More details on designing parameters  $\alpha$  and  $\beta$  are available in [9].

$$R_{d,i,discharge} = \frac{C_{BAT,i}}{C_{max}} \alpha \cdot \exp(\beta \cdot (100 - SOC)) \quad (5)$$

The droop control strategy is implemented in a dual-loop configuration, which is provided in the next section.

### 3.1.3 Control system design

Based on the developed power management algorithm, the control system of the power converters should be designed to control the desired parameters. This deliverable focuses on design the control system for the bidirectional DC-DC storage side power converters and interlink DC-AC converters. According to the previous section, the DC-DC converter should work in both power flow direction, and both CC and CV modes. The current loop control system that regulates the inductor current (battery current) is depicted in Figure 7. The plant is the

control signal to current transfer function, and the reference current is set by power management algorithm, and the current controller is a PI (Proportional-Integrator) controller.

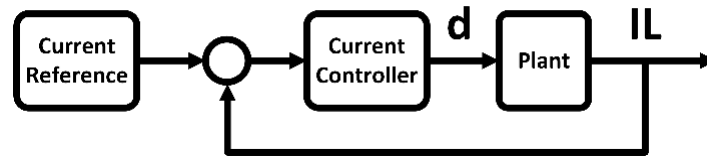


Figure 7: Current loop control for DC-DC converter

In this case, the plant is an L-filter and considering using a PI controller, the closed loop transfer function of the loop results in a second-order system [5], and can be written as:

$$G_I(s) = \frac{G_{Controller}(s) \cdot G_{Plant}(s)}{1 + G_{Controller}(s) \cdot G_{Plant}(s)} = \frac{2\zeta\omega \cdot s + \omega^2}{s^2 + 2\zeta\omega \cdot s + \omega^2} \tag{6}$$

Where,  $\zeta$  and  $\omega$  are parameters that should be designed to tune the system based on the desired BW (Band Width), Gain Margin (GM), and Phase Margin (PM). By selecting the bandwidth of the loop to one-tenth of switching frequency, which yields  $BW = 6283.2$  rad/s, and proper GM and PM, the controller coefficients can be calculated based on methods in [6]. The results are as follows:

$$K_P = 0.0079$$

$$K_I = 0.1234$$

The bode diagram for the closed-loop system and the step response are provided in Figure 8 and Figure 9, respectively. The response shows that there is no overshoot in the response and the system reaches steady state in 1ms.

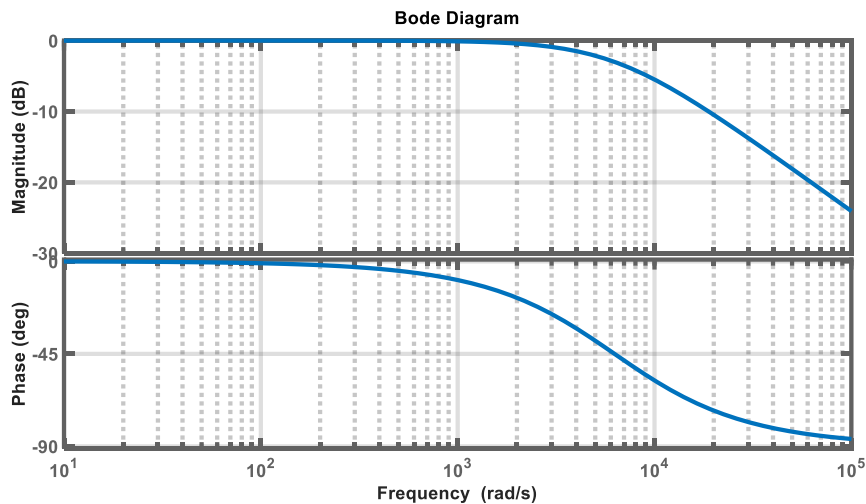
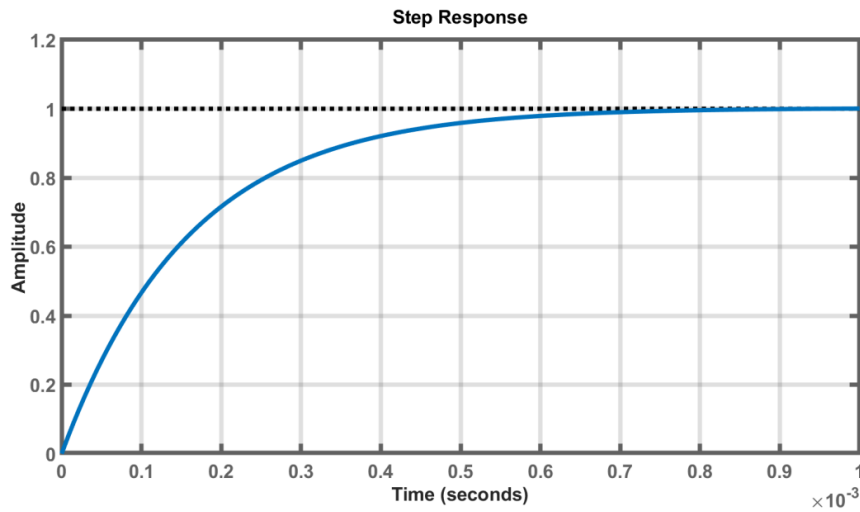
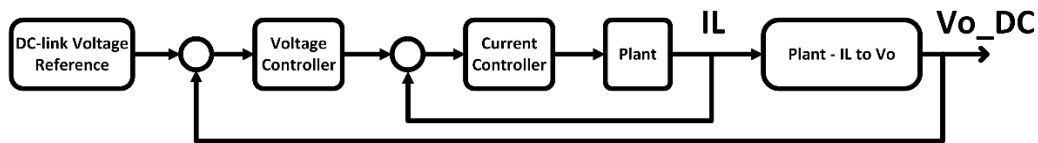


Figure 8: Closed loop bode diagram for current loop



**Figure 9: Step response of current loop control system**

In the case that the DC-DC converter is responsible for regulating the DC-link (e.g., Mode 2), a voltage loop is added to produce the reference current. The corresponding dual-loop control loop is provided in Figure 10.



**Figure 10: Dual loop control of DC-DC converter**

Inductor current to output voltage transfer function in a DC-DC boost converter can be written as:

$$G_{IL_{Vo}}(s) = \frac{R(1-D)}{R \cdot C_o \cdot s + 1} \tag{7}$$

The B.W. of the outer loop is set to be around 200 rad/s, to ensure enough decoupling with the inner loop. By tuning the inner loop properly, the loop gains of the inner loop at the desired B.W. can be ignored, and the controller can be designed. The controller coefficients for the outer loop are:

$$\begin{aligned} K_p &= 7.6532 \\ K_I &= 653.2006 \end{aligned}$$

The open loop transfer function of the dual-loop system can be obtained by:

$$G_{V_{ol}}(s) = G_{IL_{Vo}} \cdot G_I(s) \cdot C_V(s) \tag{8}$$

Where  $C_V(s)$  is the outer loop controller transfer function. The corresponding closed-loop transfer function is derived, and the bode diagram and step response are provided in Figure 11 and Figure 12, respectively. These Figures show that the outer loop is stable, and output voltage is regulated, in which the tracking constraint is satisfied, while the overshoot is limited at 20%.

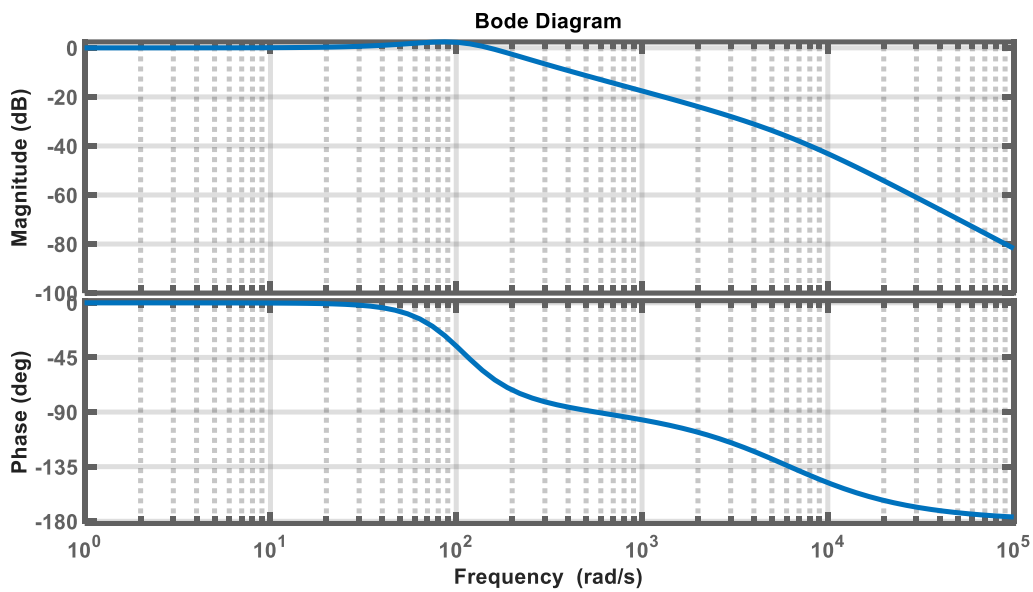


Figure 11: Closed loop bode diagram for dual loop control

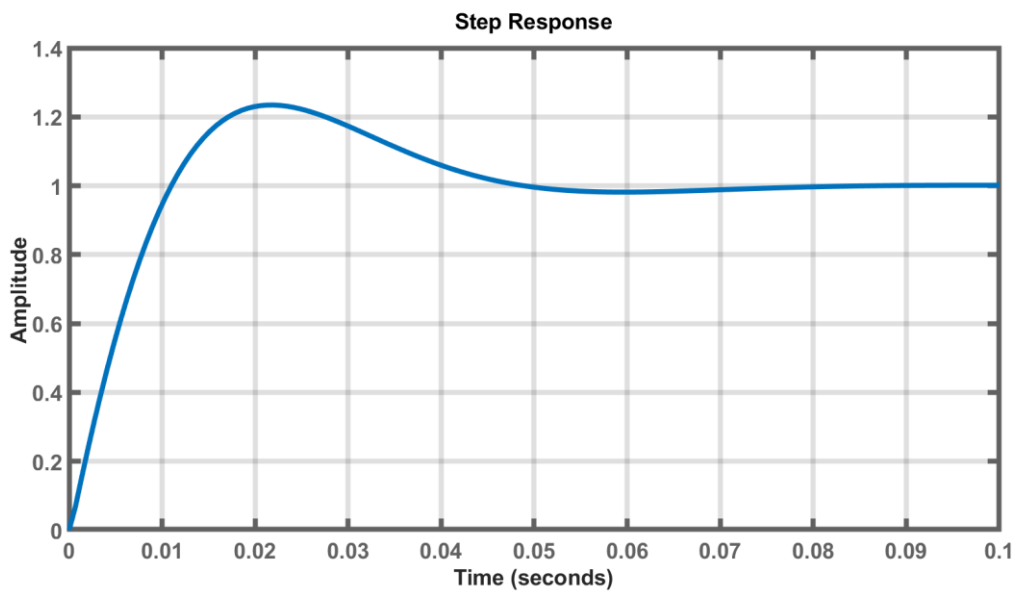


Figure 12: Step response of dual loop control system

Now that the dual-loop control system is complete, the droop strategy that is provided by PMS, is added to the loop, as shown in Figure 13.  $R_d$  is the droop coefficient which is calculated using (5).

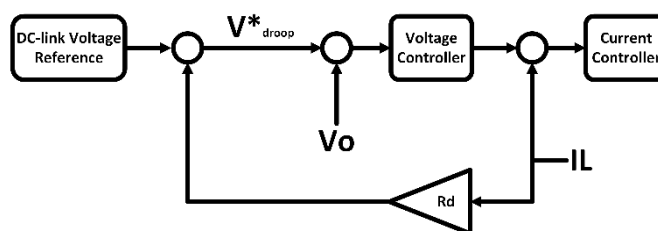


Figure 13: Dual-loop control system with droop strategy

According to the available modes in this use case, the interlink inverter/rectifier operates in various modes, including grid-following and grid-forming. In the mode that the only power generation unit in the system is the battery, the inverter controls the AC bus and the injected current to the loads. In the modes that DGs are operating, the inverter follows the AC bus to inject current to the loads and maintains the DC-link voltage. In these modes, the converter needs to operate in both directions.

In grid-following mode, the dual-loop control system for the inverter that is shown in Figure 14 is designed according to the models and equations provided in [10]. It should be noted that to synchronize the injected current with the AC bus, a Phase Locked Loop (PLL) is utilized. The phase of the system is calculated by PLL block, in which it applied to the abc-dq transformation.

First, the inner current loop is designed to set the B.W. of the current loop to be half of the resonance frequency (5.0265e+03 rad/s). The single update mode is selected for sampling method, so the sampling time is 250  $\mu$ s. According to [10], the PI current controller coefficients are as follows.

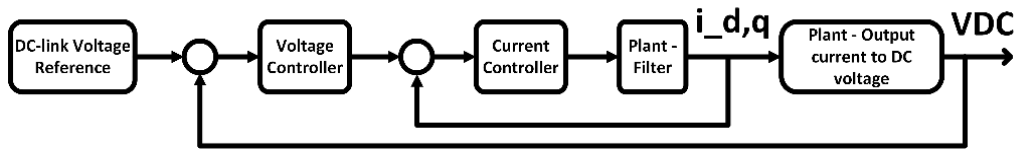


Figure 14: Dual-loop control for the inverter in grid-following mode

$$K_p = 0.0668$$

$$K_I = 15.7288$$

This yields the required B.W. (around half of the resonance frequency) for the loop while limiting the overshoot to a certain value. To attenuate the peak gain at resonance frequency, a damping resistor is added to the circuit. The value of the resistor is derived to satisfy (9).

$$|G_{ol}(s)|_{s=j\omega_{res}} = |C_c(s)G_{plant}(s)|_{s=j\omega_{res}} = 1 \text{ (0 dB)} \quad (9)$$

In which  $G_{ol}(s)$ ,  $C_c(s)$ , and  $G_{plant}(s)$ , are open-loop transfer function of inner-loop, current controller, and plant (filter) transfer function, respectively. Hence, the damping resistor is selected to be 0.0169  $\Omega$ . In this case, the current loop B.W. is set to 1.3983e+03 rad/s that is smaller than the resonance frequency. The bode diagram of the open-loop transfer function for inner-loop is provided in Figure 15. It is shown that (9) is satisfied.

To design the voltage loop and ensure stability, the required B.W. for the voltage loop is set to be one-tenth of the inner-loop, to get enough decoupling with inner-loop. By using equations in [10], the voltage loop transfer controller coefficients are as follows.

$$K_p = 4$$

$$K_I = 400$$

Corresponding bode diagram for the closed-loop system is provided in Figure 16. For the grid-forming mode, the inverter is in Voltage Controlled Mode (VCM) and regulates the output voltage and frequency. In this mode, the inner current loop is same with the grid-following mode, but the outer-loop is replaced with the ac voltage loop. The reference for VCM is set to be the same with DGs output. The PLL is also eliminated in this mode.

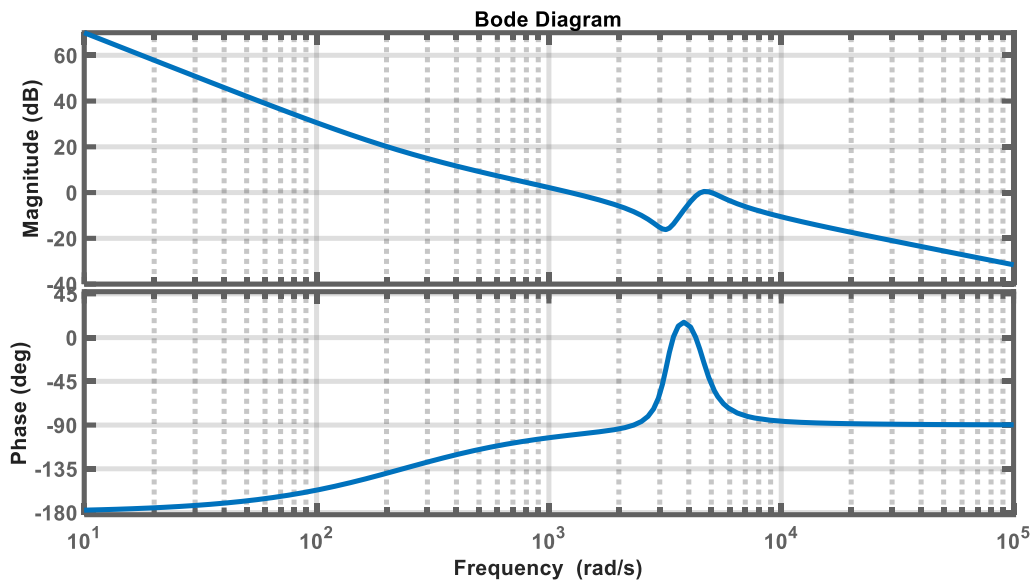


Figure 15: Bode diagram of open-loop transfer function for the inner-loop

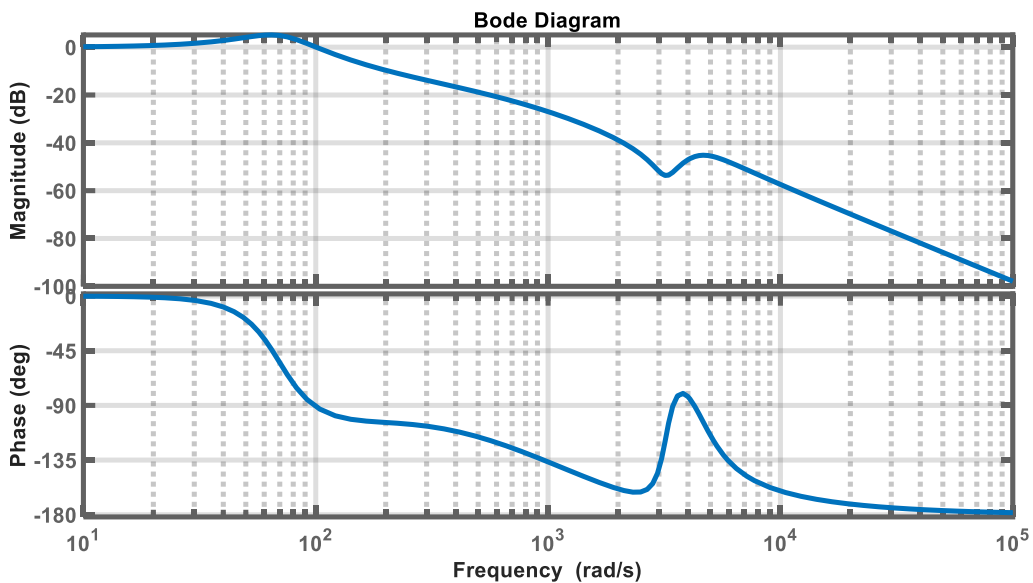


Figure 16: Bode diagram of the closed-loop system for the inverter dual loop system

Considering the dc voltage to output voltage transfer function in VCM, an integrator with the gain of 30 stabilizes the loop, ensuring desired control parameters of the system. The bode diagram and step response of the closed-loop system in VCM is provided in Figure 17 and Figure 18, respectively. It is shown that there is no overshoot in the step response for the VCM.

The controller transfer functions are converted to the z-domain in discrete form, to be implemented in the digital signal processor. The sampling time for the conversion is 250  $\mu$ s, as mentioned earlier. It should be noted that, to maintain scalability of the process in control system design, the sensor gains, and delay transfer functions are ignored, however, they are considered in final implementation in microcontrollers.

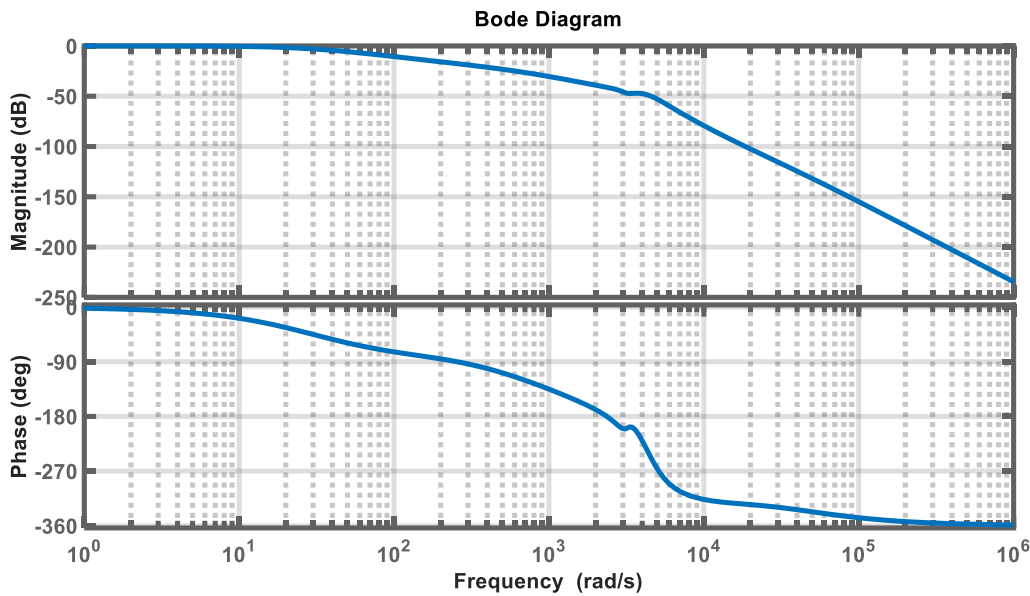


Figure 17: Bode diagram of closed-loop system in VCM

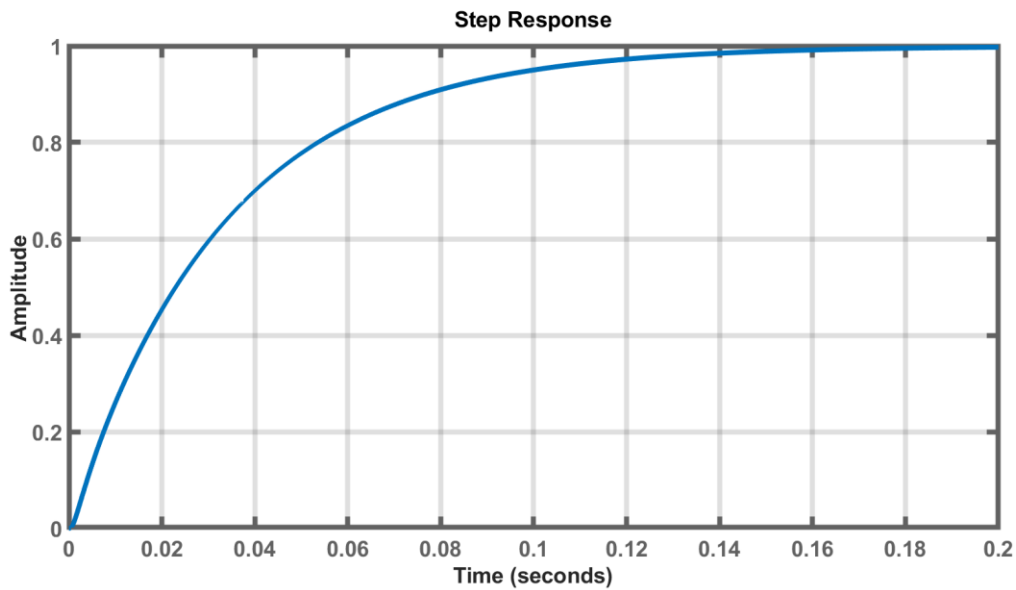
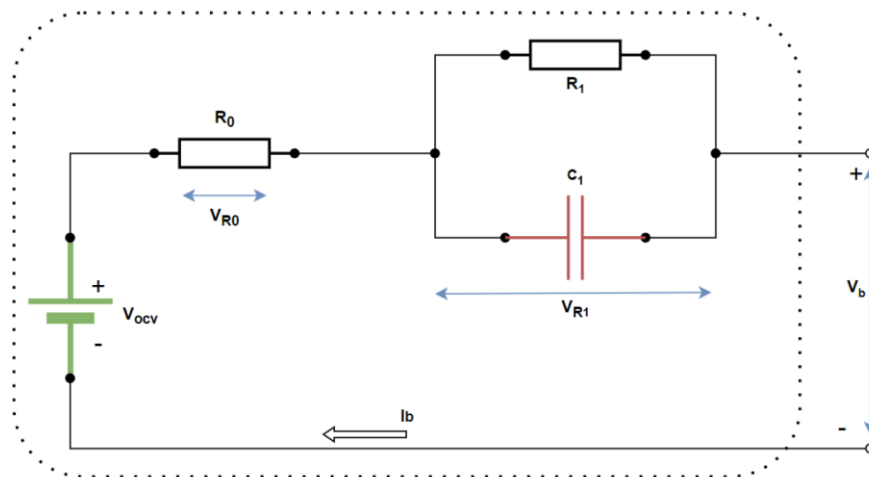


Figure 18: Step response of the closed-loop system in VCM

### 3.1.4 SSB in HIL platform

The modelling of SSB for the HIL platform is based on the validated electro-thermal models developed and discussed in D2.1-D2.2 [1], D3.1-D3.2 [2], and D4.1-4.2 [3]. These models incorporate detailed Equivalent Circuit Models (ECMs), accurately reflecting the electrical and thermal characteristics of SSB cells. The ECM framework includes open-circuit voltage ( $V_{ocv}$ ), internal resistance ( $R_0$ ), polarization resistance ( $R_1$ ), and capacitance ( $C_1$ ), which together describe the battery’s dynamic electrical response. Figure 19 provides the electrical behaviour of SSB cells, detailing key parameters such as  $V_{ocv}$ ,  $R_0$ ,  $R_1$ , and  $C_1$ , which are essential for real-time voltage and current simulations.



**Figure 19: ECM for SSB**

Figure 20 displays the heat generation and dissipation mechanisms within SSB cells, crucial for understanding thermal stability under operational conditions. Additionally, thermal modelling accounts for heat generation, dissipation, and energy losses during charging and discharging cycles. These models were parameterized using experimental data from WP3. For a detailed understanding of the modelling methodology, parameter extraction, and electro-thermal validation, refer to D2.1 [2], D3.2 [3], and D4.1 [4]. These figures, originally developed in WP2, WP3 and WP4, provide a structured visualization of the electrical and thermal modelling techniques used for HIL simulations, ensuring realistic and reliable battery behaviour within the test platform.

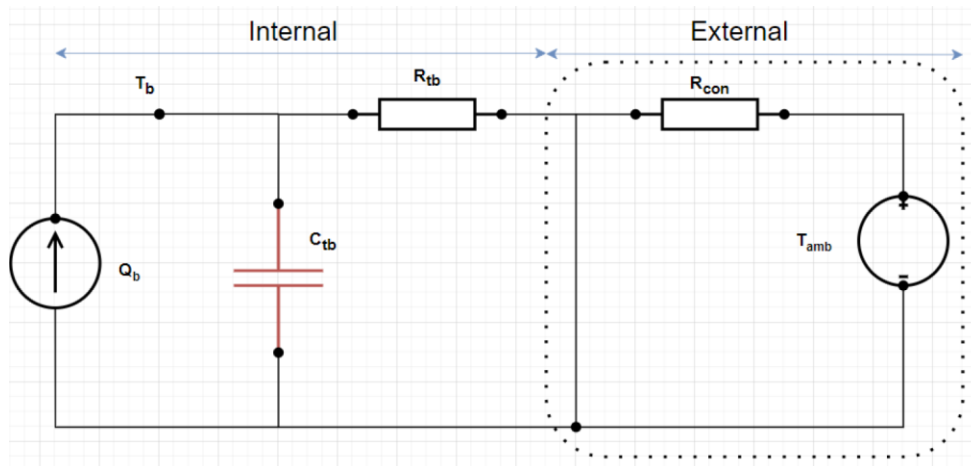


**Figure 20: Equivalent thermal model for SSB**

The same approach is utilized to model the ECM of SSB in both PSIM and Typhoon HIL environment. Figure 21 shows the detailed battery model in Typhoon HIL environment. Besides basic parameters, this model includes diffusion parameters and a thermal model as well. It should be noted that this model supports up to three pairs of RC circuits, so there is a need to convert the original five RC pairs that were developed in previous WPs to be compatible with this model. The OCV,  $R_0$ ,  $R_n$ , and  $C_n$  are two-dimensional parameters based on both SoC and cell temperature. The required data shown in Figure 21 are imported from WP3. The SSB modules consist of 308 series cells and 168 parallel cells. The data are converted to be matched with the real-time simulation environment. Accordingly, the SOC, OCV,  $R_0$ , and temperature vectors are derived.

State of charge vector:	<input type="text" value="SOC_vector"/>	P.u.	Model order:	<input type="text" value="3"/>
Initial state of charge:	<input type="text" value="SOC_init"/>	%	Resistor 1:	<input type="text" value="R1_vector"/> Ω
State of health vector:	<input type="text" value="SOH_vector"/>		Capacitor 1:	<input type="text" value="C1_vector"/> F
Temperatures vector:	<input type="text" value="Temp_vector"/>	C	Resistor 2:	<input type="text" value="R2_vector"/> Ω
Open circuit voltage:	<input type="text" value="OCV_vector"/>	V	Capacitor 2:	<input type="text" value="C2_vector"/> F
Internal resistance:	<input type="text" value="R0_vector"/>	Ω	Resistor 3:	<input type="text" value="R3_vector"/> Ω
Coulombic efficiency:	<input type="text" value="ce_vector"/>		Capacitor 3:	<input type="text" value="C3_vector"/> F
Number of cells in parallel:	<input type="text" value="N_p"/>		Temperatures vector for diffusion parameters:	<input type="text" value="0"/> C
Nominal capacity:	<input type="text" value="Total capacity"/>		State of health vector for diffusion parameters:	<input type="text" value="0"/>
Discharge capacity:	<input type="text" value="4.592, 14.532, 14.444"/>	Ah	Battery cell thermal model:	<input checked="" type="checkbox"/>
Minimum/cut-off voltage:	<input type="text" value="2.81"/>	V	Thermal resistance(s):	<input type="text" value="Tres"/> K/W
Discharge rate:	<input type="text" value="15"/>	A	Thermal capacitance(s):	<input type="text" value="Tcap"/> J/K
Total capacity:	<input type="text" value="Capacity_vector"/>	Ah	Initial cell temperature:	<input type="text" value="T0"/> C
Execution rate:	<input type="text" value="Te_cell"/>	s		

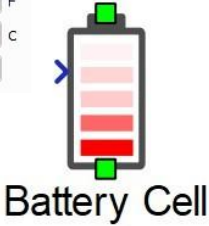


**Figure 21: Battery cell model in Typhoon HIL**

In addition, an equivalent RC network is developed to represent diffusion process parameters. This RC network consists of three resistor-capacitor (RC) pairs, where each resistor (R1, R2, R3) and capacitor (C1, C2, C3) pair models a different time constant of the battery's electrochemical behaviour. These elements capture charge transfer dynamics, voltage relaxation effects, and diffusion-induced voltage response at different time scales. Since the original model contained five RC pairs, reducing it to three requires parameter optimization to preserve accuracy while ensuring computational efficiency for real-time simulation [7].

The thermal model, including thermal resistance (Tres) and thermal capacitance (Tcap), is supported, so the parameters are calculated according to the thermal properties of the SSB cell developed in WP3. This thermal model enables the simulation of self-heating effects, heat dissipation, and temperature-dependent performance variations. Together, the electrical and thermal models ensure a complete and realistic battery representation in the Typhoon HIL environment [8].

## 3.2 Use case 2: SC

### 3.2.1 Power system design

Based on the original architecture proposed in D2.2 and D2.3 [2], the shipboard microgrid architecture and corresponding power converters and filters are designed. The overall architecture of the shipboard for UC #2 (SC) is depicted in Figure 22. The SC modules are connected to the main AC bus through bidirectional DC-DC and DC-AC converters. The DC-DC converter is utilized because SC output voltage decreases while it is discharging. So, the DC-DC converter provides stable output voltage for the DC-AC converter. It should be noted that based on the optimization results in D2.3, it is considered that the SC module is connected to the AC bus, and whole energy is going to the load side with a single module. So, the simulation model is developed to be aligned with the optimization results in D2.3.

Diesel generators and shaft generators are feeding the main AC bus, based on the PMS/EMS command. The main AC bus voltage is 690V, based on the original design of the shipboard power system. The battery packs output voltage is in the range of 900V to 1.1kV (based on the corresponding SoC), which is directly connected to the main AC bus via inverters.

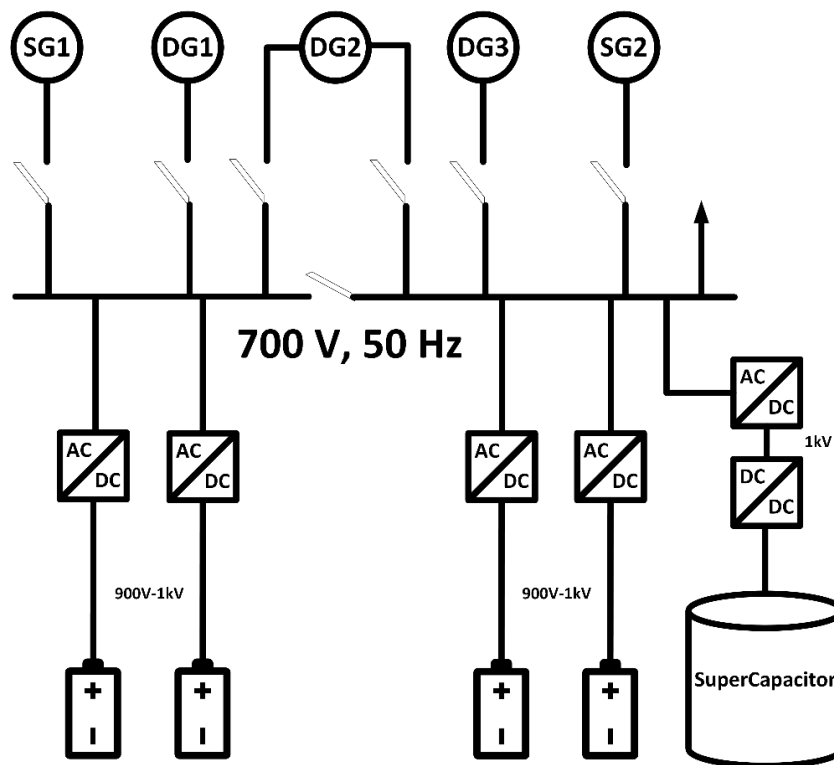


Figure 22: Shipboard microgrid for UC#2 (SC)

Next, according to the load profile and required power and energy, the power rating of the shipboard microgrid components is determined. As this project focuses on storage side solutions, it focuses on DC-DC and DC-AC storage side power converters. Based on the solutions in D2.3, required needed capacity considering largest period is 38kWh for SC module, resulting in maximum power of 2099kW. So, the power rating for DC-DC power converter is 2.1MW to deliver the required energy from SC to the load in the desired period. For this purpose, a bidirectional DC-DC converter is selected that is shown in Figure 23. In a realistic case, this DC-DC converter is a modular converter utilizing more IGBT legs. However, the operational characteristics remain the same.

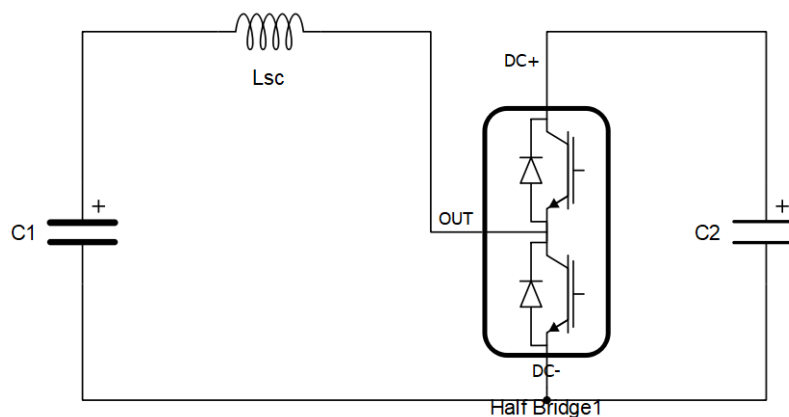


Figure 23: Bidirectional DC-DC converter with SC module

The input parameters to design the DC-DC converter are provided in Table 3.

**Table 3: DC-DC converter specifications for UC#2**

Parameter	Value
SC minimum output voltage (V)	500
SC maximum output voltage (V)	1000
DC-link Voltage (V)	1000
Output power (kW)	2100
Inductor current ripple (%)	6
Maximum voltage ripple (%)	1
Switching frequency (kHz)	8

By calculating the maximum inductor current ( $I_{L,max}$ ) and output current ( $I_o$ ) by

$$I_{L,max} = \frac{P_o}{V_{SSB,min}} \quad (10)$$

$$I_o = \frac{P_o}{V_{dc}} \quad (11)$$

where,  $P_o, V_{SC,min}, V_{dc}$ , are the output power, minimum voltage of SC, and DC-link voltage, respectively. Hence, the inductance and capacitance values can be determined:

$$L = \frac{V_{dc} \cdot D}{\Delta I_L \cdot f_{sw}} = 198.41 \mu H \quad (12)$$

$$C = \frac{D \cdot I_o}{V_{ripple} \cdot f_{sw} \cdot V_{dc}} = 10 mF \quad (13)$$

where,  $\Delta I_L, V_{ripple}, D$ , are inductor maximum current, DC-link maximum voltage ripple, and duty cycle of the power converter, respectively.

Next step is to design the three-phase interlink inverter/rectifier that is connected between the DC link and the main AC bus. This converter utilizes an LCL filter in the output, to filter out the harmonics and ensure the controllability of the converter. The input parameters to design the LCL filter is provided in Table 4.

**Table 4: DC-AC converter specifications for UC#2**

Parameter	Value
AC bus frequency (Hz)	50
RMS line-line voltage (V)	690
Input DC voltage (V)	1000
Output power (kW)	2100
Maximum output current THD (%)	5
Minimum power factor	0.995
Switching frequency (kHz)	8
Resonance frequency (kHz)	2

The LCL filter is designed to attenuate the harmonics and achieve desire current ripple reduction while limiting the AC voltage drop and maintaining high power factor. To ensure stability, the resonance frequency is set to one-fourth of the switching frequency, and the passive damping method is used in this case. This design is a reciprocal process, so the initial

values are re-calculated in a few iterations to reach the proper values within the constraints. The three-phase LCL filter is provided in Figure 24, in which the  $L_1$  is converter side inductor,  $L_2$  is the grid side inductor,  $C_f$  is filter capacitor, and  $R_d$  is damping resistor.

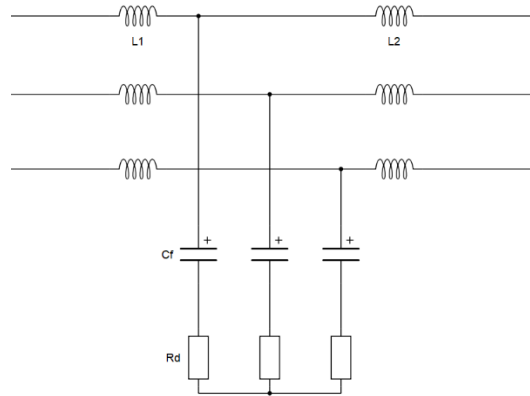


**Figure 24: LCL filter with passive damping resistance**

The calculated values for the LCL filter are as follows:

$$\begin{aligned}
 L_1 &= 18.041 \mu H \\
 L_2 &= 18.041 \mu H \\
 C_f &= 702.01 \mu F \\
 R_{d\_min} &= 0.0227 \Omega
 \end{aligned}$$

As the damping resistor is crucial in the control system stability, the final value for the damping resistor is calculated in the process of controller design in the next section.

### 3.2.2 Power Management System

The operational scenarios are an essential part for design the control system for the HIL platform. According to the power generation units that is depicted in Figure 25, different operational cases can be determined.

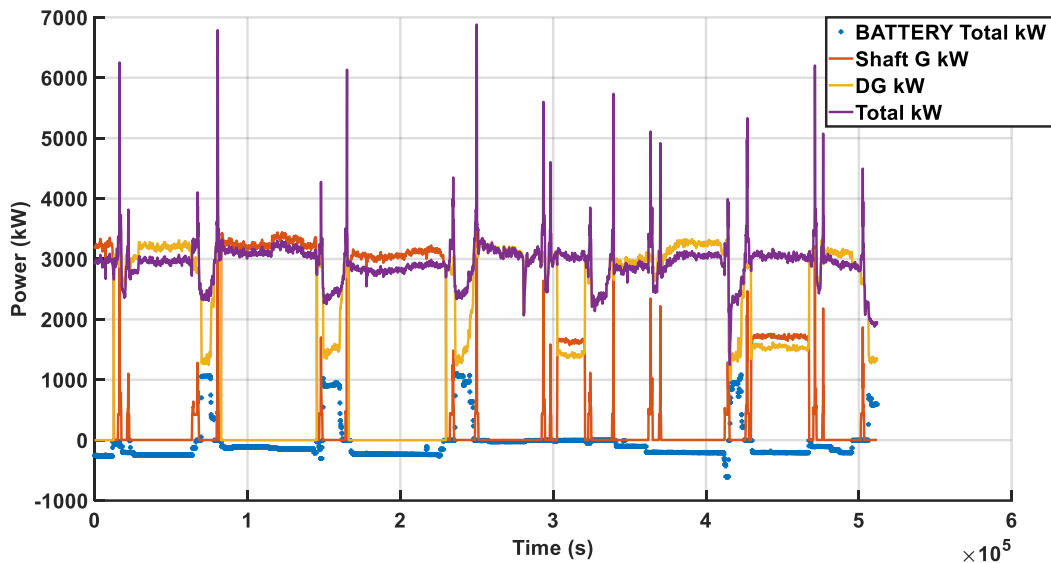


**Figure 25: Power generation units for UC#2**

SC module is responsible to operate in manoeuvring phases, where the power demand is at its peak value, as shown in Figure 25. By focusing on periods where the SC is involved, the following conditions are observed:

- Battery is the only generation source; the battery DC-AC converter is in VCM.
- Battery is discharging alongside the diesel generators and/or shaft generators; the DC-AC converter is controlling the discharging current, based on output current.

In all desired cases, the SC is the supporting unit to handle the maximum of needed power. So, PMS needs to determine the charging and discharging periods, based on the SoC and power generation status of the system, and set the reference values accordingly. Therefore, when SC is in discharging mode, the SC side DC-DC converter regulates DC output voltage and limiting the injected current, and DC-AC converter regulates injected current from SC to the load. In charging mode, DC-DC converter controls charge current of SC, and the DC-AC converter regulates DC-link voltage.

Hence, the PMS is designed to switch between charge/discharge cycles in response to the peak demand. The SC will be charged before manoeuvring phases to 100% and discharged at constant current or constant power rate. Once the SC SoC goes below 40%, it will be charged again to 100%. An advanced EMS can optimize this pattern in an efficient way to ensure that the SC provides peak demand power in desired periods.

### 3.2.3 Control system design

Based on the developed PMS, the control system of the power converters should be designed to control the desired parameters. This deliverable focuses on design the control system for the bidirectional SC side DC-DC and DC-AC converters.

According to the previous section, the DC-DC converter should work in both power flow direction, and both constant current and constant power modes. The current loop control system that regulates the inductor current (SC current) is depicted in Figure 26. The plant is the control signal to current transfer function, and the reference current is set by power management algorithm, and the current controller is a PI controller.

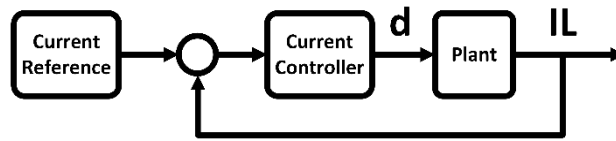


Figure 26: Current loop control for DC-DC converter

As mentioned in section 3.1.3, the closed loop transfer function of the loop, which is a second-order system can be written as:

$$G_I(s) = \frac{2\zeta\omega \cdot s + \omega^2}{s^2 + 2\zeta\omega \cdot s + \omega^2} \tag{14}$$

By selecting BW = 6283.2 rad/s, and proper GM and PM, the controller coefficients can be calculated as follows:

$$K_P = 0.0012$$

$$K_I = 0.0196$$

As the control parameters of the second-order system of current-loop are almost the same with previous design in UC#1, the bode diagram for the closed-loop system and the step response are same and provided in Figure 27 and Figure 28, respectively. The response shows that there is no overshoot in the response and the system reaches steady state in 1ms.

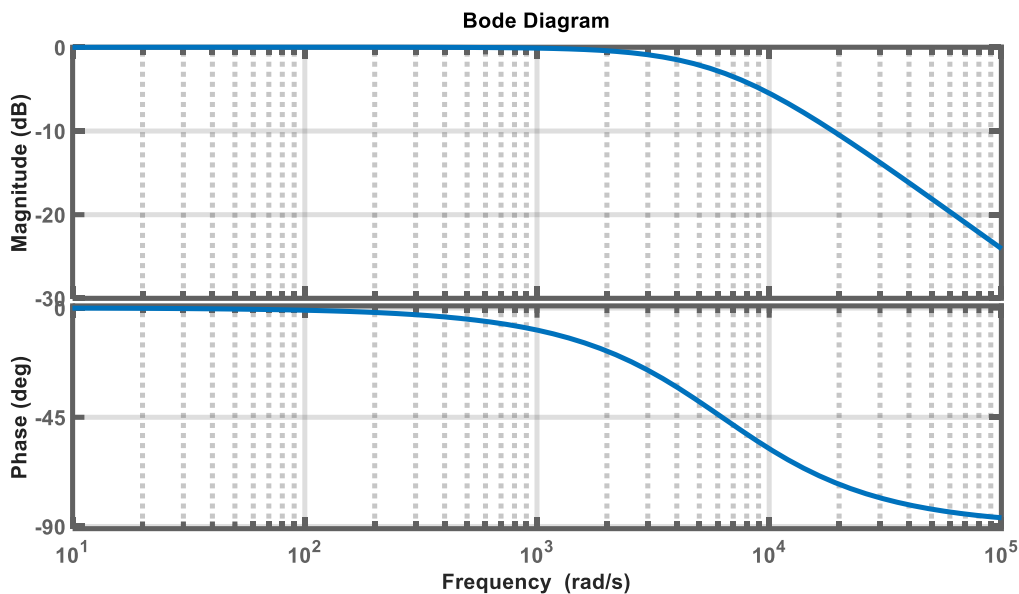


Figure 27: Closed loop bode diagram for current loop

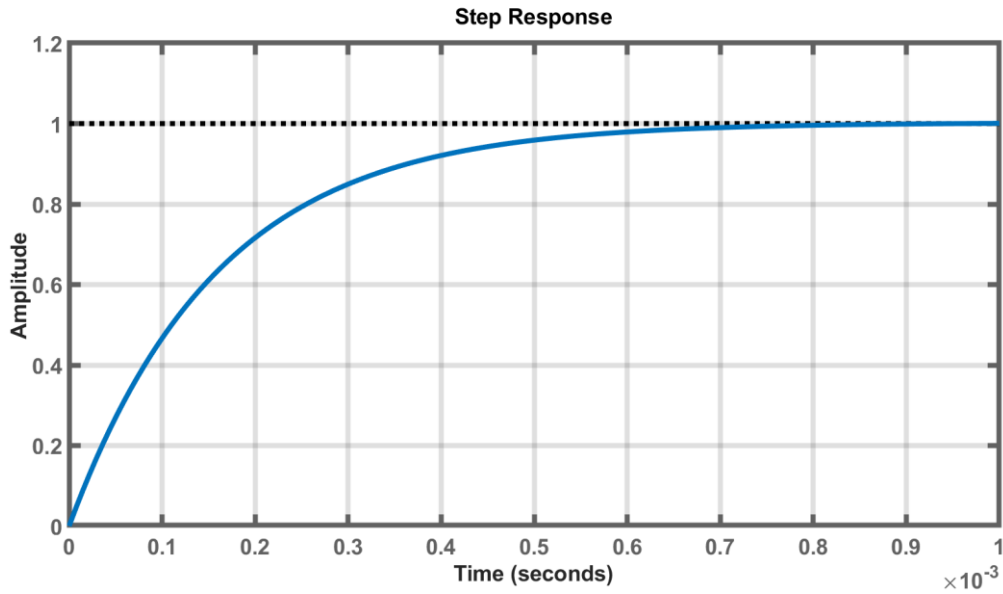


Figure 28: Step response of current loop control system

As the DC-DC converter is responsible for regulating the DC-link, a voltage loop is added to produce the reference current. The corresponding dual-loop control loop is provided in Figure 29. In the case that there is no need to regulate the DC-link voltage (charging mode), outer loop can be eliminated, and the PMS set the reference current directly.

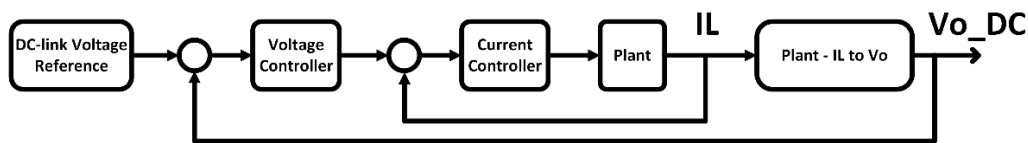


Figure 29: Dual loop control of DC-DC converter

Inductor current to output voltage transfer function in a DC-DC boost converter can be written as:

$$G_{IL_{Vo}}(s) = \frac{R(1-D)}{R \cdot C_o \cdot s + 1} \tag{15}$$

The B.W. of the outer loop is set to be around 314 rad/s, to ensure enough decoupling with the inner loop. By tuning the inner loop properly, the loop gains of the inner loop at the desired B.W. can be ignored, and the controller can be designed. The controller coefficients for the outer loop are:

$$K_p = 2.6887$$

$$K_I = 1.5374e + 03$$

The open loop transfer function of the dual-loop system can be obtained by:

$$G_{V_{ol}}(s) = G_{IL_{Vo}} \cdot G_I(s) \cdot C_V(s) \tag{16}$$

where  $C_V(s)$  is the outer loop controller transfer function. The corresponding closed-loop transfer function is derived, and the bode diagram and step response are provided in Figure 30 and Figure 31, respectively. These Figures show that the outer loop is stable, and output

voltage is regulated, in which the tracking constraint is satisfied, while the overshoot is limited at 15%.

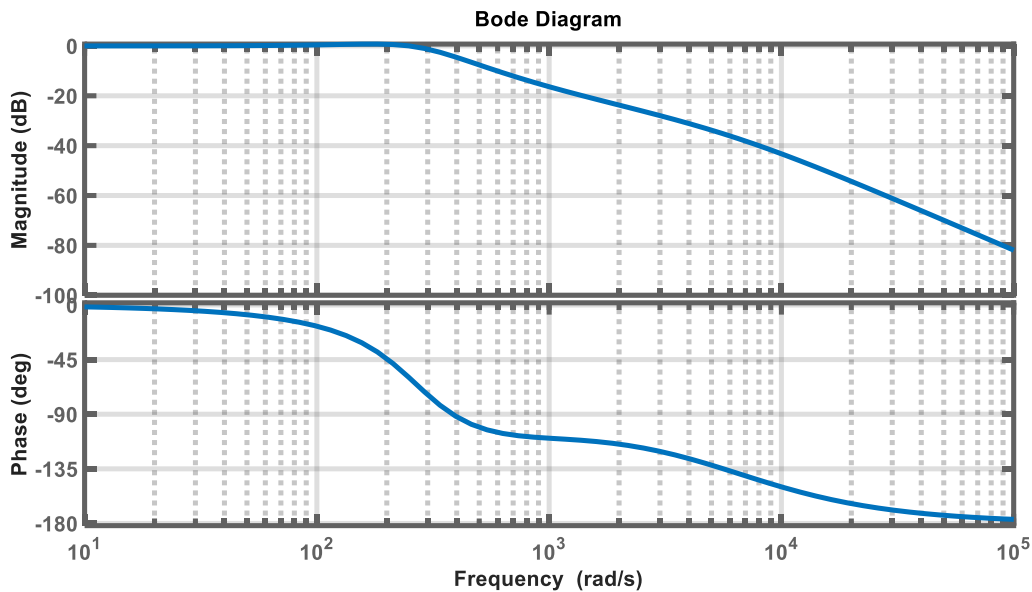


**Figure 30: Closed loop bode diagram for dual loop control**

The DC-AC converter operates in grid-following mode and follows the AC bus to inject current to the loads and maintains the DC-link voltage. In these modes, the converter needs to operate in both directions.

In grid-following mode, the dual-loop control system for the inverter that is shown in Figure 32 is designed according to the models and equations provided in [10]. It should be noted that to synchronize the injected current with the AC bus, a Phase Locked Loop (PLL) is utilized. The phase of the system is calculated by PLL block, in which it applied to the abc-dq transformation.

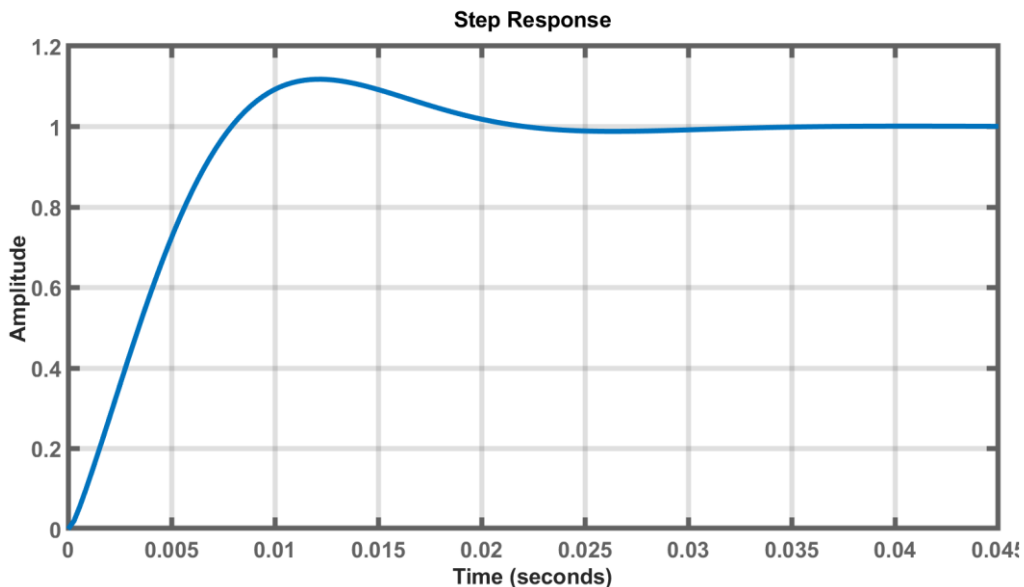


**Figure 31: Step response of dual loop control system**

First, the inner current loop is designed to set the B.W. of the current loop to be half of the resonance frequency (1.2566e+04 rad/s). The double update mode is selected for sampling

method, so the sampling time is 62.5 μs. According to [10], the PI current controller coefficients are as follows.

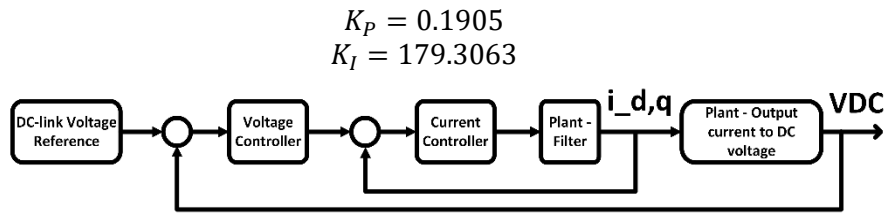


Figure 32: Dual-loop control for the inverter in grid-following mode

This yields the required B.W. (around half of the resonance frequency) for the loop while limiting the overshoot to a certain value. To attenuate the peak gain at resonance frequency, a damping resistor is added to the circuit. The value of the resistor is derived to satisfy (17).

$$|G_{ol}(s)|_{s=j\omega_{res}} = |C_c(s)G_{plant}(s)|_{s=j\omega_{res}} = 1 \text{ (0 dB)} \tag{17}$$

where  $G_{ol}(s)$ ,  $C_c(s)$ , and  $G_{plant}(s)$ , are open-loop transfer function of inner-loop, current controller, and plant (filter) transfer function, respectively. Hence, the damping resistor is selected to be 0.0521 Ω. In this case, the current loop B.W. is set to 5.0281e+03 rad/s that is smaller than the resonance frequency. The bode diagram of the open-loop transfer function for inner-loop is provided in Figure 33. It is shown that (17) is satisfied.

To design the voltage loop and ensure stability, the required B.W. for the voltage loop is set to be one-tenth of the inner-loop, to get enough decoupling with inner-loop. By using equations in [10], the voltage loop transfer controller coefficients are as follows.

$$K_P = 3.3600$$

$$K_I = 1344$$

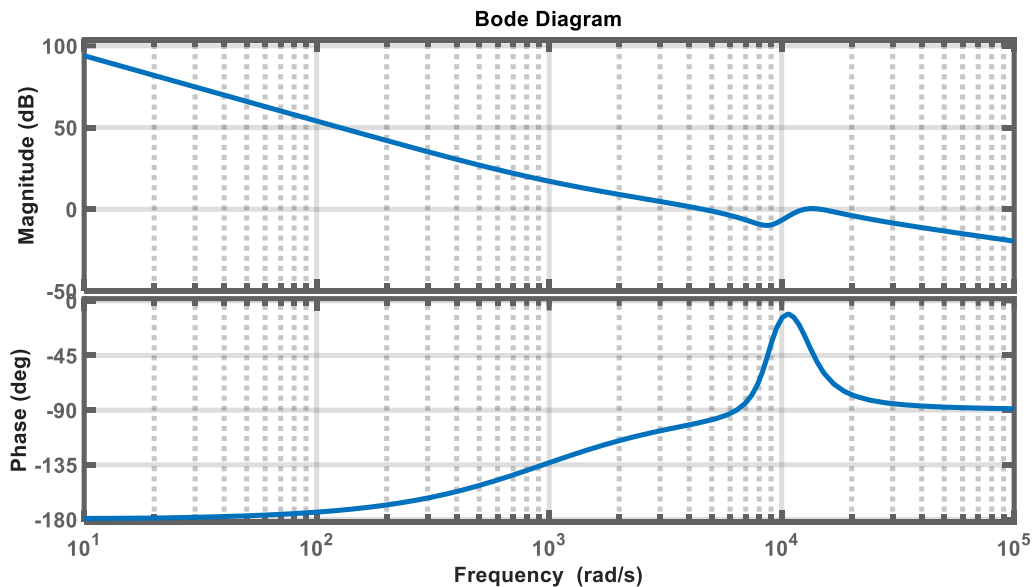


Figure 33: Bode diagram of open-loop transfer function for the inner-loop

Corresponding bode diagram for the closed-loop system is provided in Figure 34.

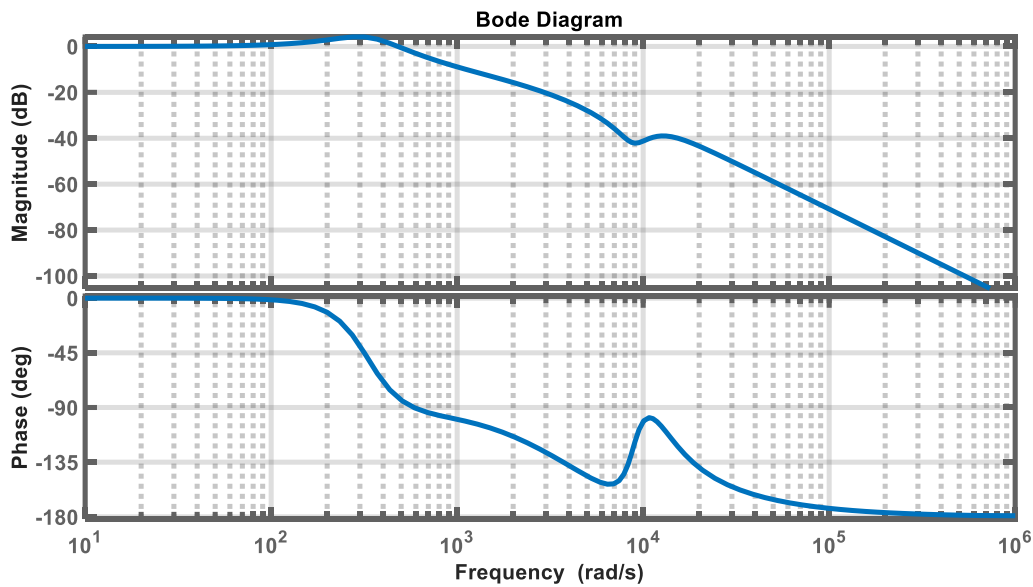
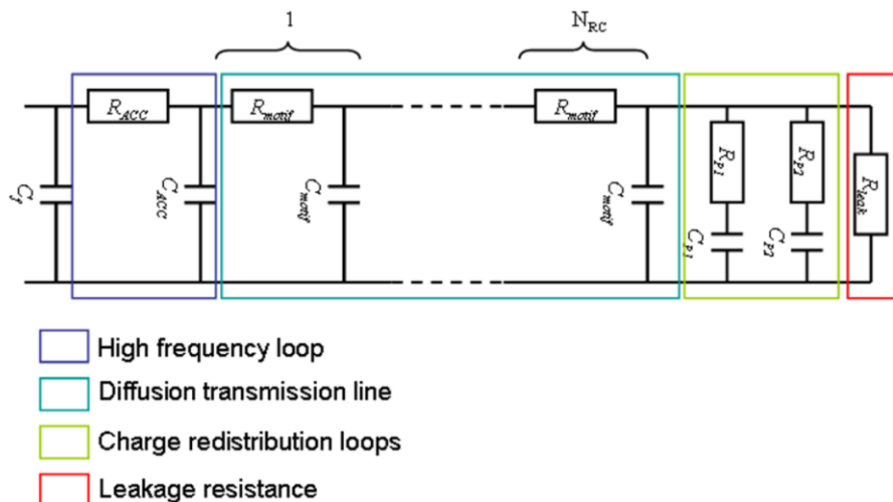


Figure 34: Bode diagram of the closed-loop system for the inverter dual loop system

The controller transfer functions are converted to the z-domain in discrete form, to be implemented in the digital signal processor. The sampling time for the conversion is 62.5 μs, as mentioned earlier. It should be noted that, to maintain scalability of the process in control system design, the sensor gains, and delay transfer functions are ignored, however, they are considered in final implementation in microcontrollers.

### 3.2.4 SC in HIL platform

The SC modeling for HIL implementation is based on electrochemical and ECM approaches developed and simulated in D2.1, D3.2 and D4.2 as shown in Figure 35. The loop in the violet box consists of  $R_{ACC}$  and  $C_{ACC}$  and represents high-frequency phenomena. The cyan box consists of  $N_{RC}$  elements, which represent the diffusion transmission line, the two next branches are for charge redistribution phenomenon, and red box includes the leakage resistance. The electrical parameters of this circuit are temperature dependent  $R_{motif}$  and/or voltage dependent ( $C_{motif}$ ,  $R_{P1}$ ,  $C_{P1}$ ). The supercapacitor model with parasitic element is selected in Typhoon HIL environment to emulate the characteristics of the developed SC module in WP3.



**Figure 35: Dynamic SC phenomena modelled with an ECM**

In the characterization process of the SC, the following key variables are used.

- Capacitive energy storage characteristics: SC models incorporate double-layer capacitance, equivalent series resistance ( $E_{SR}$ ), and leakage resistance.
- Charge-discharge dynamics: SC voltage and current response are modeled, considering fast transient behavior, variable capacitance, and charge redistribution effects.
- Thermal modeling: Electro-thermal models estimate heat dissipation, efficiency losses, and thermal response under dynamic loads.

### **3.3 Use case 3: Hybrid ESS (SSB and SC)**

#### **3.3.1 Power system design**

In this use case, there is no original architecture for the shipboard power system. The main goal of this UC is to replace diesel generators with SSB and SC modules. Considering results in D2.3, the shipboard microgrid architecture and corresponding power converters and filters are designed. The overall architecture of the shipboard for UC #3 is depicted in Figure 36. The SSB and SC modules are connected to the main AC bus through bidirectional DC-DC and DC-AC converters.

Shaft generators are feeding the main AC bus, based on the PMS/EMS command. The main AC bus voltage is 400V, based on the original design of the shipboard power system.

Next, according to the load profile and required power and energy, the power rating of the shipboard microgrid components is determined. As this project focuses on storage side solutions, it focuses on DC-DC and DC-AC storage side power converters. Based on the solutions in D2.3, required needed capacity for battery is 1566 kWh, resulting in maximum power of 505 kW. And 49 kWh is required for SC module, which results in a 1912 kW module.

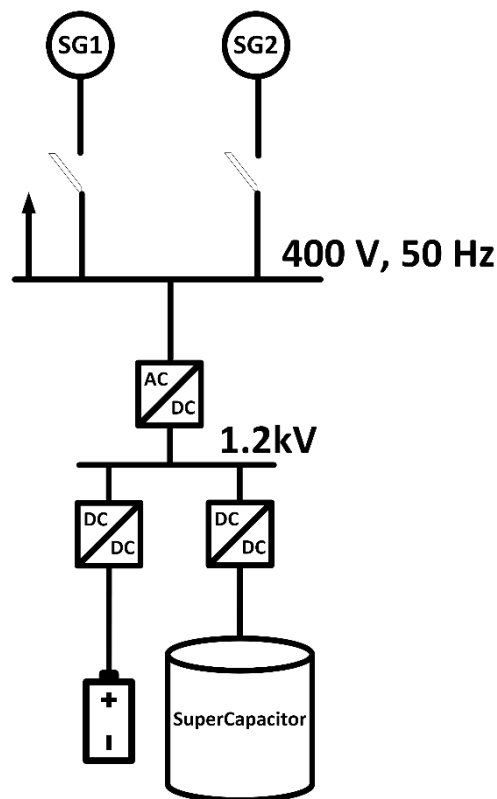


**Figure 36: Shipboard microgrid for UC#3**

So, the power rating for SSB DC-DC, SC DC-DC, and DC-AC converters are 500 kW, 2MW, and 2.5MW, respectively. According to the equations (10)-(14), and [10], the design is done similar to the previous use cases., and the results are as follows.

$$\begin{aligned}
 L_{dc\_SSB} &= 693.75 \mu H \\
 L_{dc\_SC} &= 362.5 \mu H \\
 C_{dc\_link} &= 10 mF \\
 L_1 &= 18.041 \mu H \\
 L_2 &= 18.041 \mu H \\
 C_f &= 702.01 \mu F \\
 R_{d\_min} &= 0.0064 \Omega
 \end{aligned}$$

As the damping resistor is crucial in the control system stability, the final value for the damping resistor is calculated in the process of controller design in the next section.

### 3.3.2 Power Management System

As there is no specific load profile in this use case, the PMS is designed based on basic operation of a hybrid ESS, in which the SSB is providing the required power to the main AC bus, and SC is the supporting unit during manoeuvring for peak demand. So, the SSB DC-DC and SC DC-DC converters regulate SSB and SC output currents, and the inverter is controlling DC-link voltage and output current. When shaft generator is disconnected, the inverter is in grid-forming mode and controls the output voltage, and SSB DC-DC converter controls the DC-link voltage.

### 3.3.3 Control system design

The control system design for all the possible control loops is provided in previous sections. As the loop and control strategies for both SSB and SC modules are the same, the final design values of control system are provided in this section based on the parameters of UC#3. First, the controller coefficients for current loop control of SSB DC-DC converter are:

$$K_P = 0.0036$$

$$K_I = 0.0571$$

And the controller coefficients for current loop of SC DC-DC converter are:

$$K_P = 0.0019$$

$$K_I = 0.0298$$

As the SSB DC-DC converter is responsible for regulating the DC-link in some cases, a voltage loop is added to produce the reference current. The corresponding dual-loop control loop is provided in Figure 37. In the case that there is no need to regulate the DC-link voltage (charging mode), outer loop can be eliminated, and the PMS set the reference current directly.

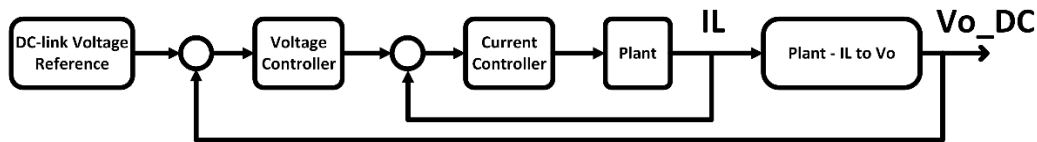


Figure 37: Dual loop control of DC-DC converter

The controller coefficients for the outer loop are:

$$K_P = 2.6887$$

$$K_I = 1.5374e + 03$$

The corresponding bode diagram and step response are provided in Figure 38 and Figure 39, respectively. These Figures show that the outer loop is stable, and output voltage is regulated, in which the tracking constraint is satisfied, while the overshoot is limited at 15%.

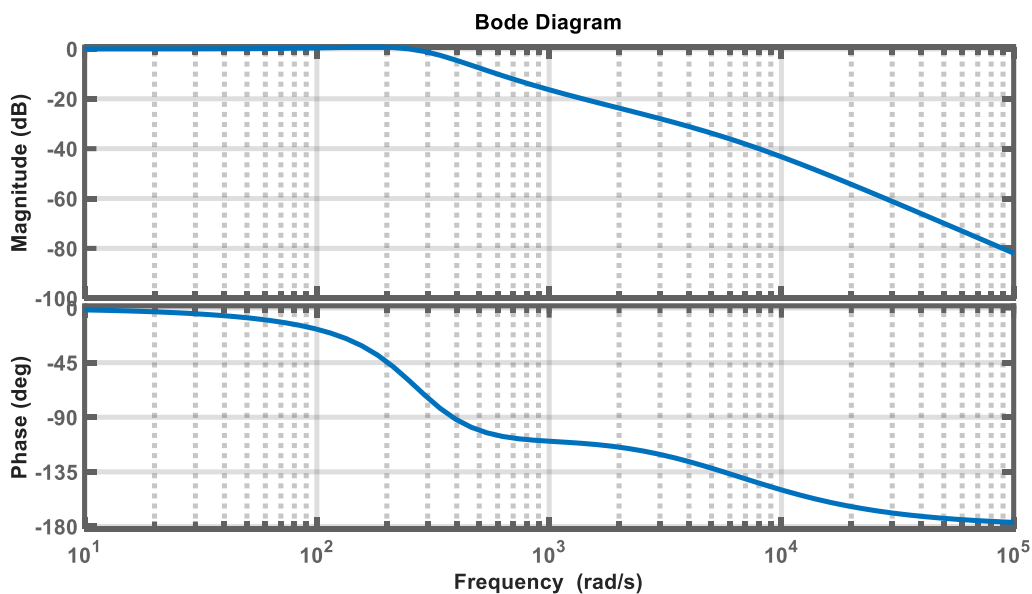
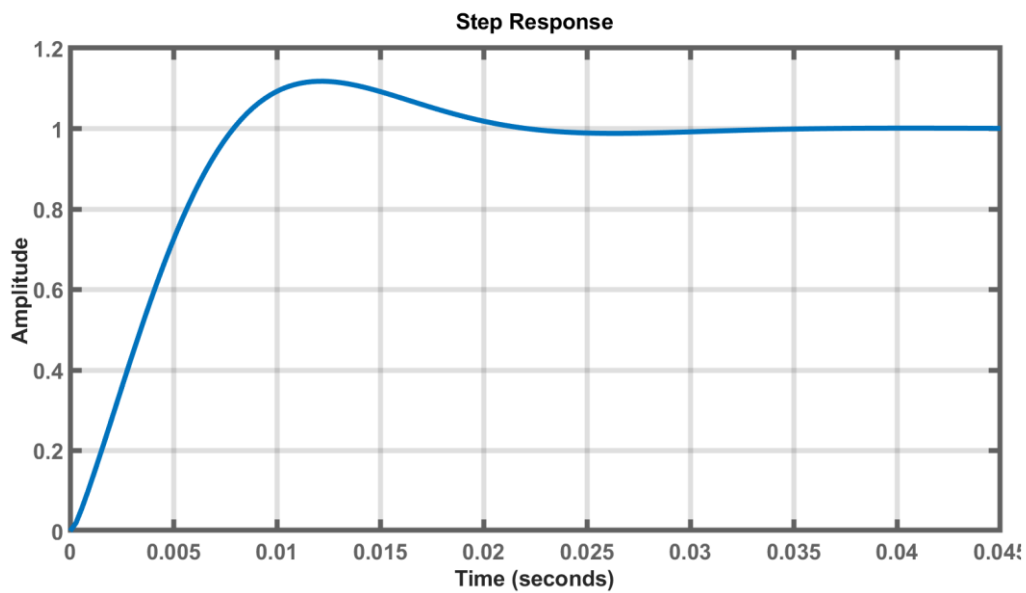


Figure 38: Closed loop bode diagram for dual loop control



**Figure 39: Step response of dual loop control system**

When the DC-AC converter operates in grid-following mode, according to [10], the PI current controller coefficients are as follows.

$$K_P = 0.0168$$

$$K_I = 3.9545$$

By using equations in [10], the voltage loop transfer controller coefficients are as follows.

$$K_P = 0.8400$$

$$K_I = 84$$

Corresponding bode diagram for the closed-loop system is provided in Figure 40.

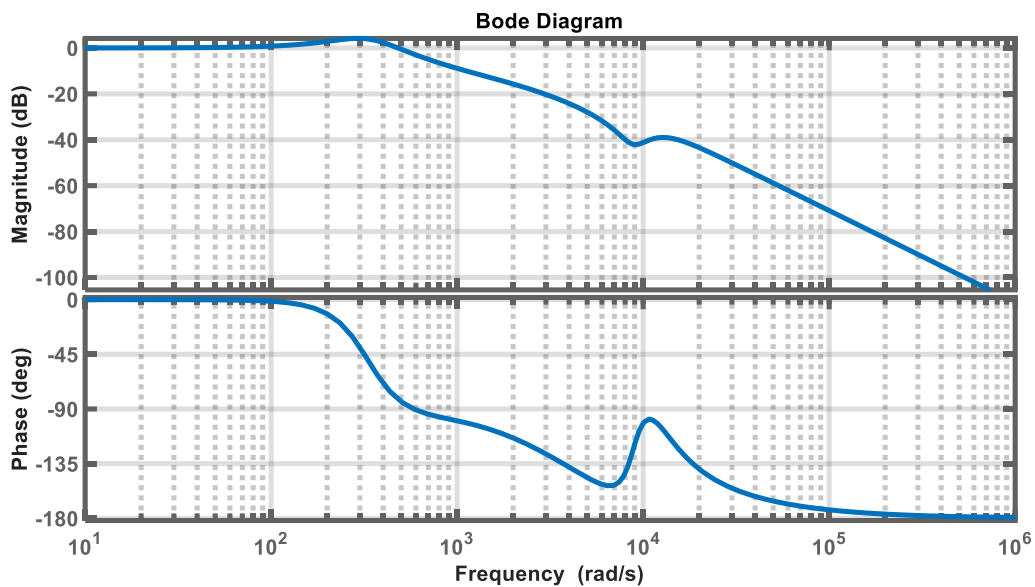


**Figure 40: Bode diagram of the closed-loop system for the inverter dual loop system**

The controller transfer functions are converted to the z-domain in discrete form, to be implemented in the digital signal processor. The sampling time for the conversion is 62.5 μs, as mentioned earlier. It should be noted that, to maintain scalability of the process in control

system design, the sensor gains, and delay transfer functions are ignored, however, they are considered in final implementation in microcontrollers.

## 4 Real-time Simulation Setup

This section introduces the setup that is developed to perform real-time simulation for introduced use cases. In this work, Typhoon HIL real-time simulator is used to simulate the power stage, and dSPACE MicroLabBox and TI C2000 DSP are used to implement control system and PMS. The overall setup is provided in Figure 41.



Figure 41: CHIL Setup

The power stages that are developed in section 3 is implemented in Typhoon HIL device. As the results of this task is a basis for the further experimental tests in T5.2, the switching behaviour of power devices with desired time step to cover fast transients should be considered. This enables more reliable models that can represent the real power devices. On the other hand, due to the limitation of computational power of real-time simulator, only a part of the power system can be modelled in each simulation.

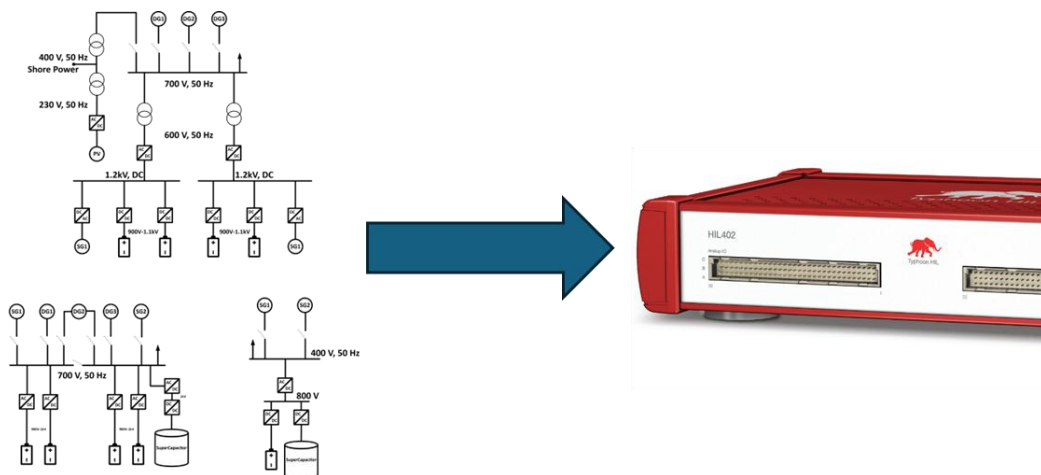
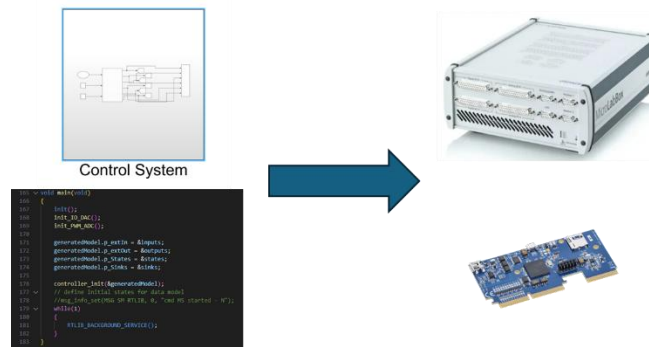


Figure 42: Shipboards microgrids and Typhoon HIL device

Therefore, based on the complexity of the power system, time step is selected to be a few microseconds (different values for different use cases) to capture fast transients, while simulating a reasonable part of the shipboard microgrid.

As shown in Figure 42, the shipboard microgrid including ESS modules, power converters, filters, transformers, and loads are implemented in Typhoon HIL device. The control system and PMS including digital controllers, PMS strategy, and PWM modulations are implemented in TI C2000 DSP and dSPACE MicroLabBox, which are shown in Figure 43.



## 5 HIL simulation results

### 5.1 Use case 1

The real-time simulation is done for various modes of the system, as defined in section 3.1.2. The HIL SCADA of real-time simulation for UC#1 is provided in Figure 45, in which every measured parameter in the shipboard microgrid can be monitored, and desired changes in setpoints and loads can be applied to check the effectiveness of control system. For example, the reference current for SSB modules, SoC, shaft generator ON/OFF and its injected current to the system, and DG ON/OFF can be changed separately to watch the effects on stability of the system. It should be noted that due to the computational limitations of real-time HIL devices, it is not possible to simulate the whole power system based on Figure 2. To maintain the accuracy of the simulation, two SSB modules with one single DC-AC interlink converter is studied in this simulation. The shaft generator and its AFE rectifier is considered as a dynamic current source. The other half of the system performs the same, so the model keeps its scalability.

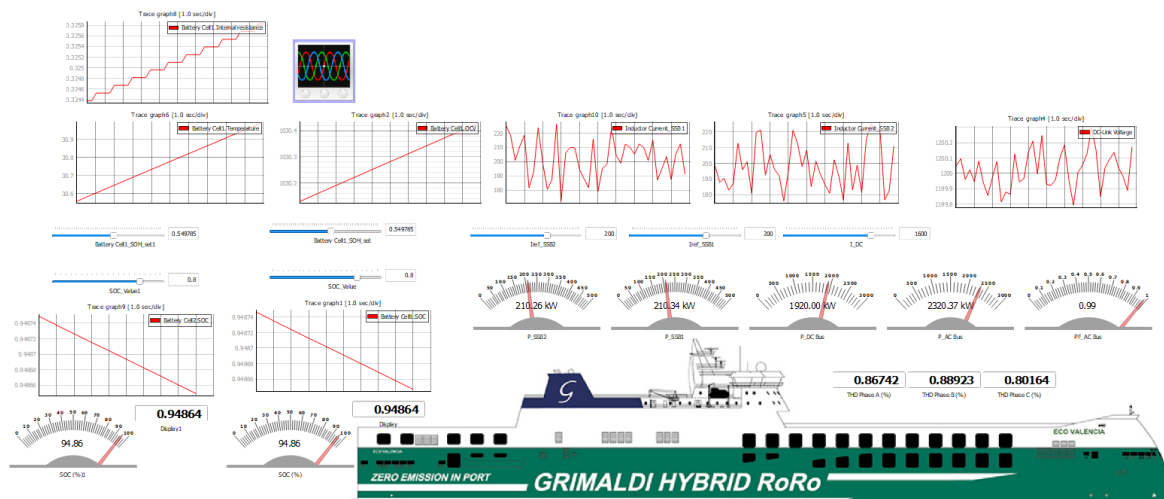
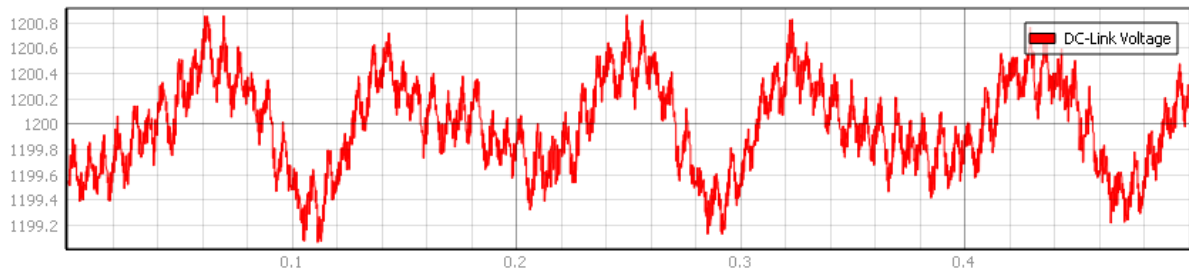


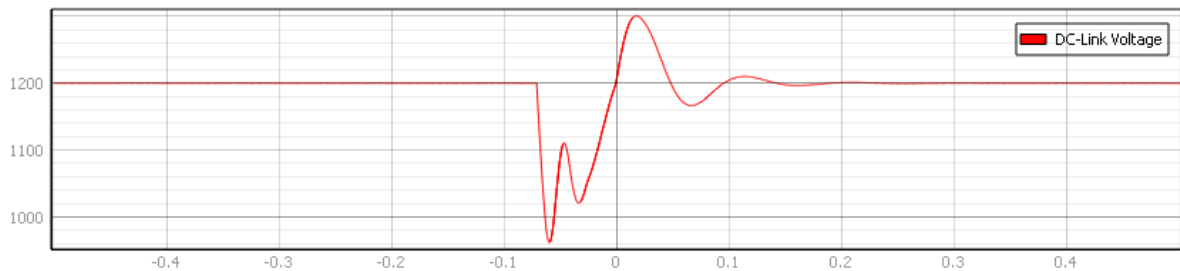
Figure 45: HIL SCADA for UC#1

To validate the control system of SSB modules in different modes, the real-time simulation performed for scenarios that SSB modules are involved. First, the results for discharging modes, including mode 3 (SSB + DG), mode 7 (SSB + SG + DG), and mode 2 (only SSB) are provided. Next, a long-term simulation is performed in real-time with actual timeframe to validate the system performance in both discharging and charging modes.

Figure 46 shows the DC-link voltage in steady state, when the inverter is controlling the DC-link, for both modes 3 and 7. Figure 47 verifies the stability of the control system in switching from mode 7 to mode 3, when the shaft generator is disconnected in the system. So, the system remains stable, while the SSB are the only generation units in the DC side of the microgrid.

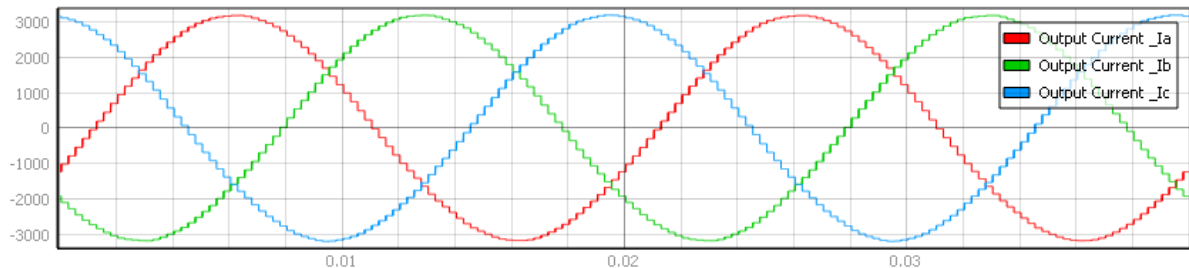


**Figure 46: Steady state DC-link voltage waveform in real-time simulation in mode 3 and mode 7**



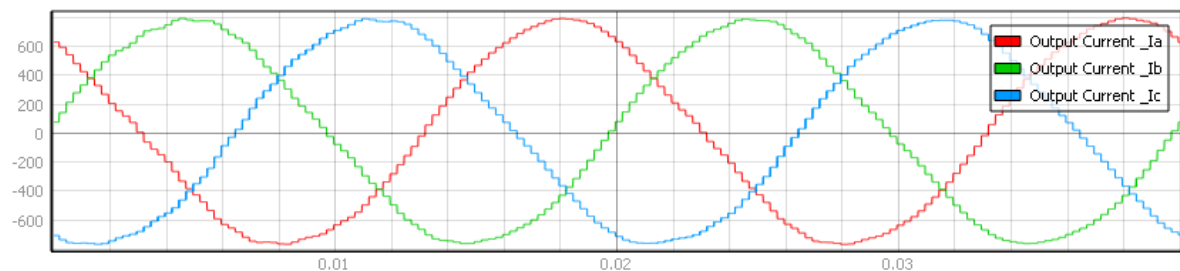
**Figure 47: DC-link voltage in transition from mode 7 to mode 3**

The inverter output current waveforms in mode 7 is provided in Figure 48. For this case, the THD of the waveform is 0.8%. In this mode, the inverter is working at its full load operation.



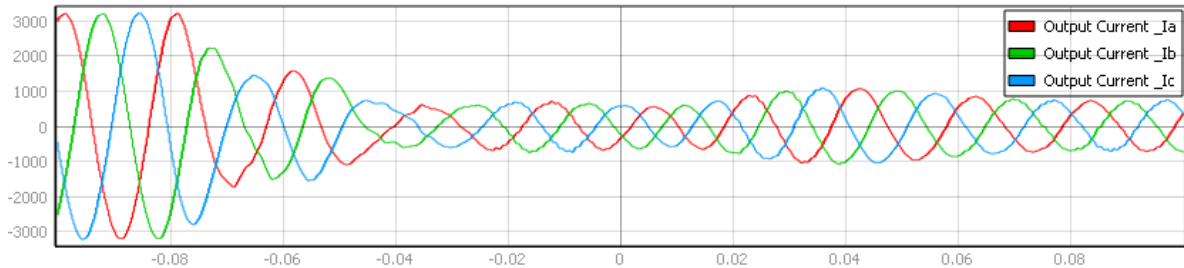
**Figure 48: Inverter output currents in mode 7**

Figure 49 shows the inverter output currents in mode 3, when the inverter is working at about 0.25 of its full-load capabilities with only SSB units. The THD in this condition is 3.3%. As expected, the THD increased due to the lower current level at the fundamental frequency.



**Figure 49: Inverter output currents in mode 3**

The transition between mode 7 and mode 3 is depicted in Figure 50. As expected, the inverter currents decreased to the lower level, due to the disconnection of shaft generator. However, the inverter regulates the current to the desired value.



**Figure 50: Inverter output currents in transition between mode 7 and mode 3**

For both modes 3 and 7, the DC-DC converters are responsible to control the SSB current and injected power to the AC bus. The reference current for the converter inductor is set to 180A, to inject 188kW to the AC side that is their full-load capability. As shown in Figure 51, SSB modules are injecting the desired current.

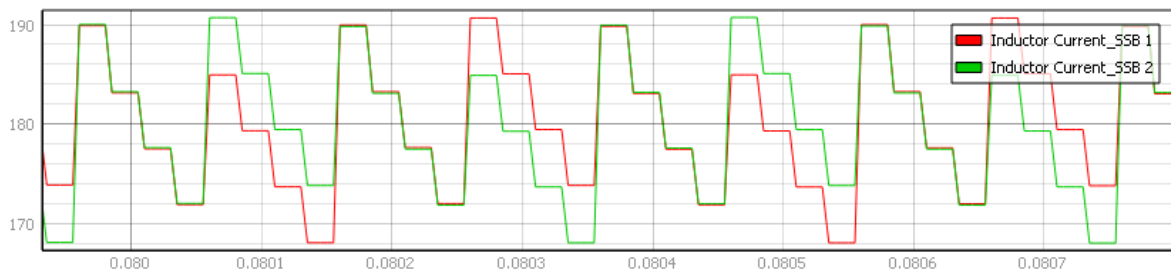


**Figure 51: Output current of SSB1 and SSB2 at 180A for modes 3 and 7**

In mode 2, where the SSB modules are the only generation sources and are in grid-forming state, the DG and SG are disconnected, so the inverter is controlling the output voltage. Figure 52 shows the AC bus voltage and output voltage of the inverter, where the loads are connected. The amplitude of the phase voltage is matched with the desired design. In this case,  $Z_g = 0.9 \Omega$  as the load is connected to the AC bus. The injected current to the load is depicted in Figure 53, and the THD is 0.7%.

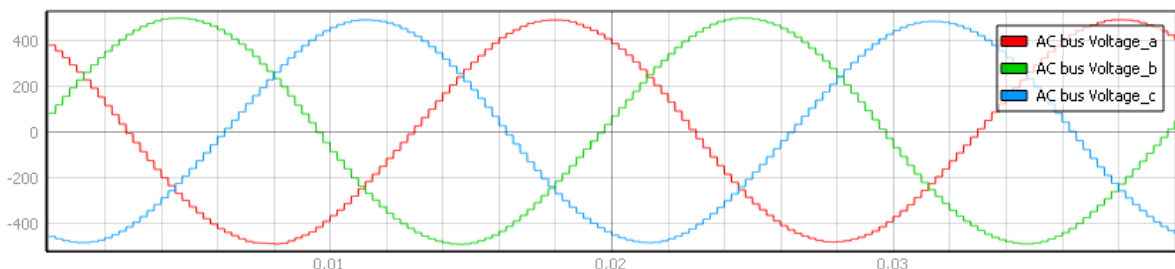


**Figure 52: Steady state output voltage waveform in real-time simulation in mode 2**

In grid-forming mode (mode 2), as the DC-DC converters are operating in dual-loop voltage mode to regulate DC-link voltage, there is a need for a power (current) sharing algorithm. Therefore, the droop strategy is selected, as it is described in section 3. In this case scenario,

the droop strategy is activated to balance the load sharing between SSB modules, while regulating the DC-link voltage.

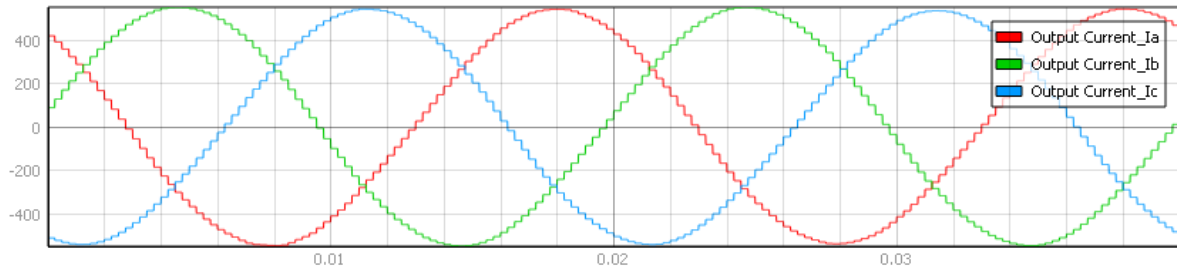


**Figure 53: Steady state output current waveform in real-time simulation in mode 2**

The DC-link voltage and SSB currents are shown in Figure 54 and Figure 55, respectively. As expected, there is a voltage drop across the DC-link voltage, so the DC voltage is decreased to 1178V. The SSB modules provides their current share for the required load current to supply the load with  $Z_g = 0.9 \Omega$ . Figure 55 shows that the current is balanced between SSB modules.

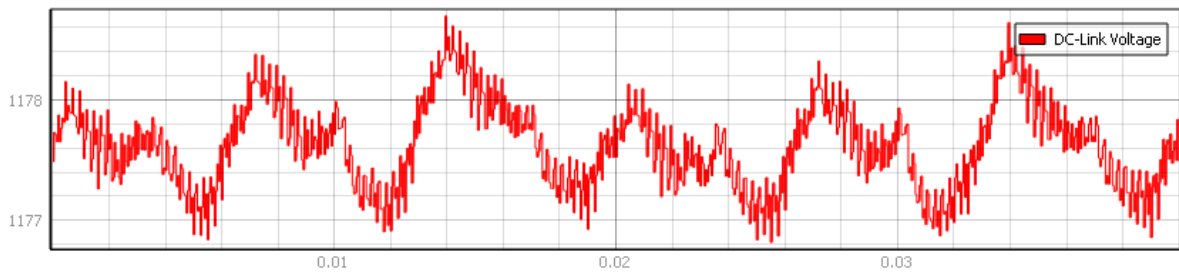


**Figure 54: Steady state DC-link voltage waveform in real-time simulation in mode 2**

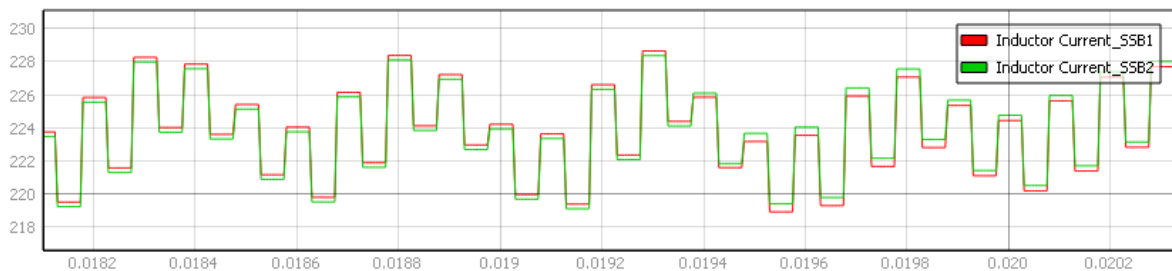


**Figure 55: Steady state SSB current waveforms in real-time simulation in mode 2**

To validate the operation of the SSB in the shipboard microgrid, a real-time simulation for 6 hours performed. The electrical signals waveform remains stable, as expected. The temperature, SoC, and output power of both SSB modules of the system are recorded in the 6-hours simulation. The output power and SoC of the modules are provided in Figure 56 in 60s sampling rate. After 2 hours, one of the SSB modules is disconnected. After 5 hours, both SSB modules switches to charging mode, so the SoC starts to increase and the output power that is show in the figure is the charging power. In the same scenario, the temperature corresponding temperature of cells with 10s sampling rate is provided in Figure 57. The long-term oscillations of the temperature results need to be verified with expected values and other long-term simulation results in Simcenter Amesim or any other simulation platform.

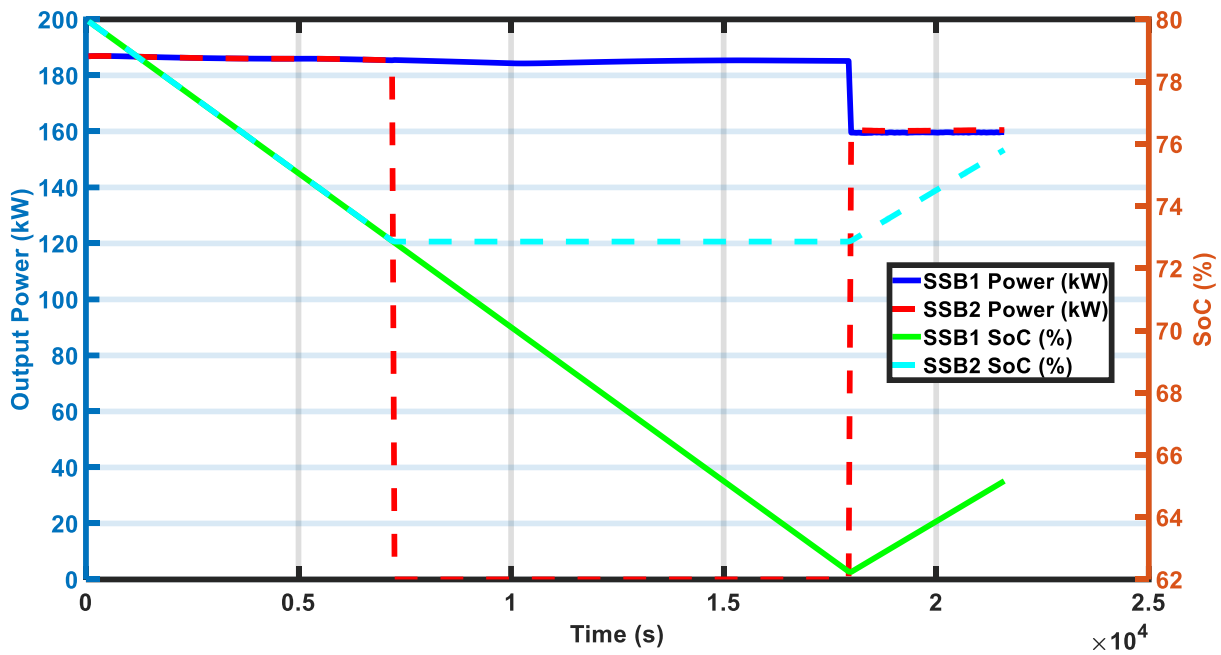


Figure 56: Output power and SoC of SSB1 and SSB2 during 6-hour simulation

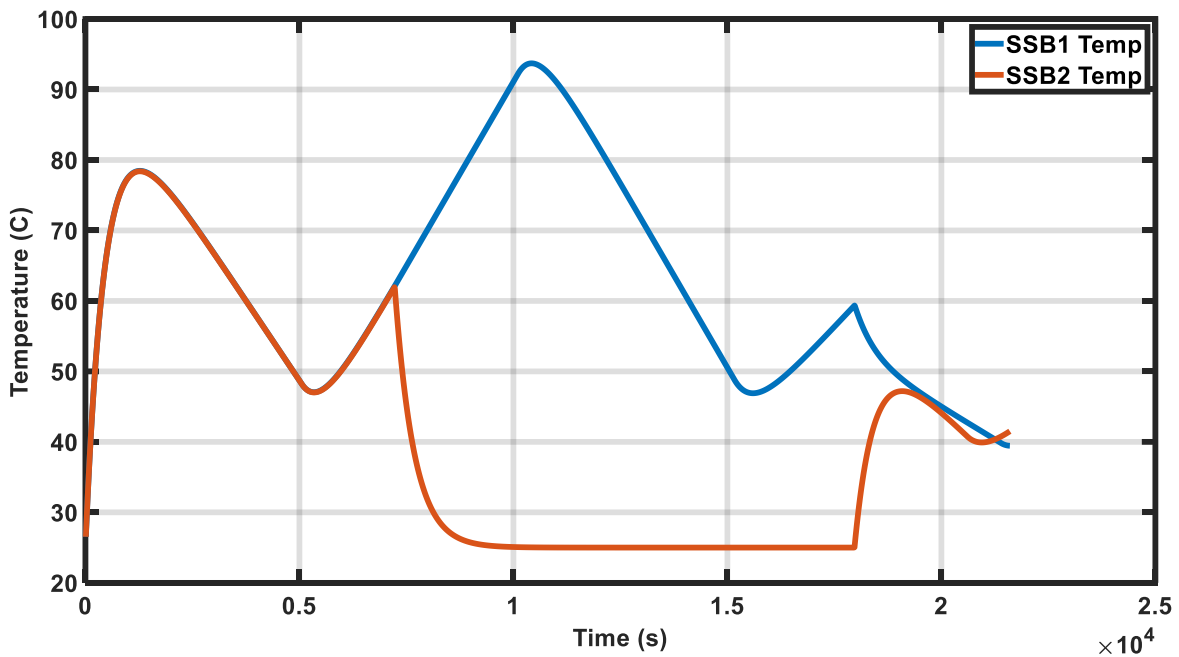
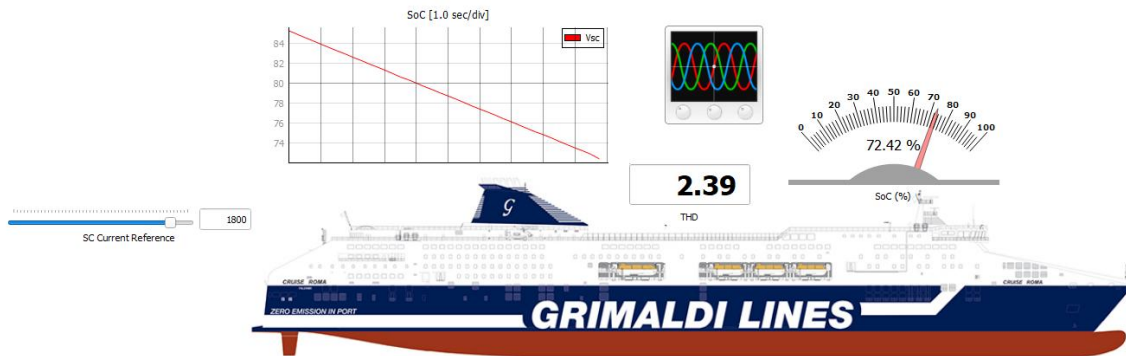


Figure 57: Output power and SoC of SSB1 and SSB2 during 6-hour simulation

## 5.2 Use case 2

The real-time simulation for UC#2 is done to show the performance of the SC charging/discharging operation in the designed system. The HIL SCADA of real-time simulation for UC#2 is provided in Figure 58, in which it includes parameters related to SC operation including SoC, SC current reference, and THD of output current. Also, it is possible to connect/disconnect SG/DG/battery and their injected current to the system separately to watch the effects on stability of the system.

It should be noted that due to the computational limitations of real-time HIL devices, it is not possible to simulate the whole power system based on Figure 22. To maintain the accuracy of the simulation, SC module with DC-DC and DC-AC converter, and the battery pack is studied in this simulation. The DG and/or SG and its AFE rectifier is considered as a dynamic current source.



**Figure 58: HIL SCADA for UC#2**

To validate the control system in charging and discharging modes, the real-time simulations were performed. First, the results in charging mode are provided in the following. Figure 59 shows the DC-link voltage of DC-DC converter that regulates the voltage at 1000V. In this case the charging current is set to 1800A. The supplied current to the SC is depicted in Figure 60. The charging current in AC side that is provided by battery and/or DG/SG is provided in Figure 61.

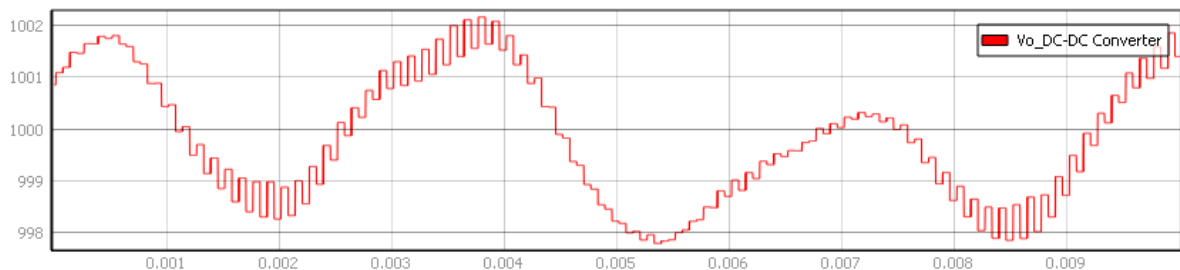


**Figure 59: Steady state DC-link voltage waveform in real-time simulation in SC charging mode**

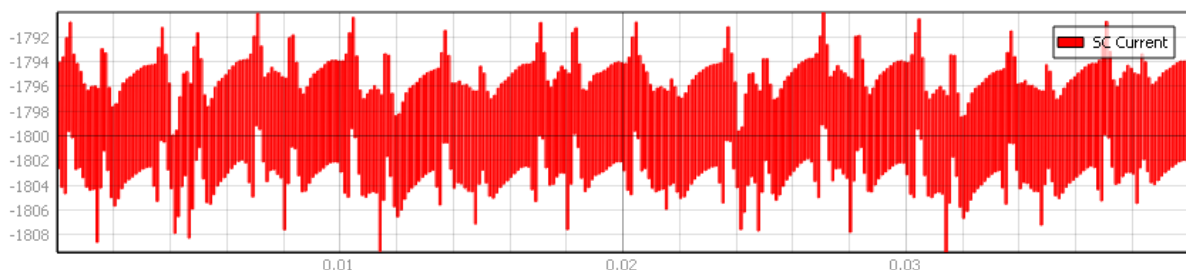


**Figure 60: Steady state SC current waveforms in real-time simulation in SC charging mode**

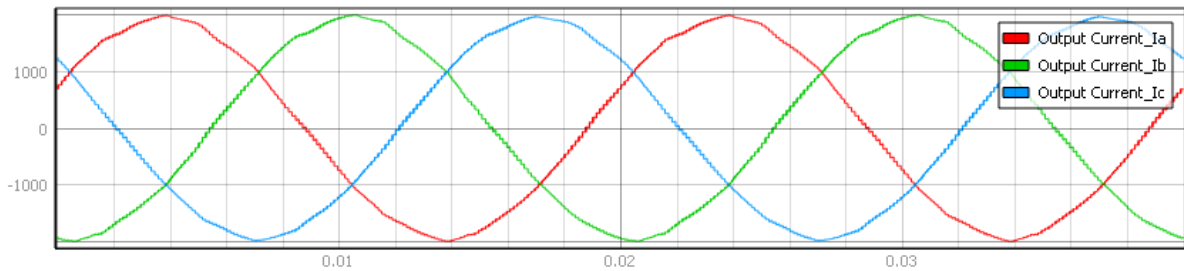


**Figure 61: Steady state AC side current waveform in real-time simulation in SC charging mode**

DC-link voltage of DC-DC converter, discharging current, and output current in the discharging mode are provided in Figure 62, Figure 63, and Figure 64, respectively.

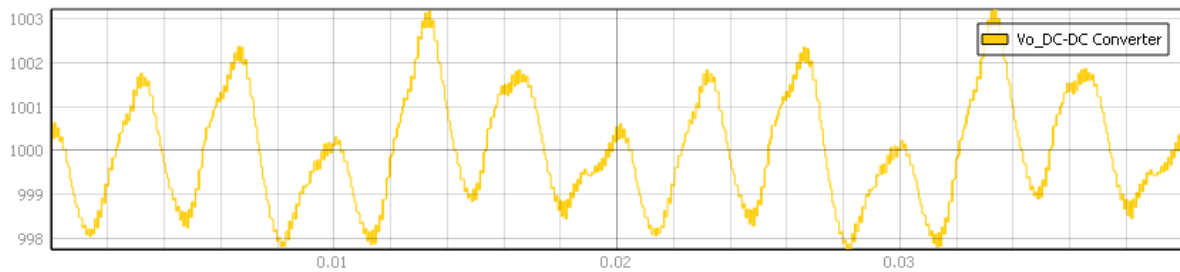


**Figure 62: DC-link voltage waveform in real-time simulation in SC discharging mode**

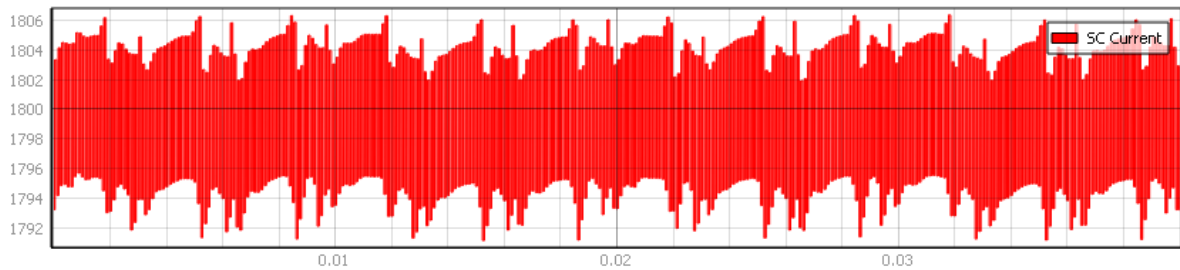


**Figure 63: SC current waveform in real-time simulation in SC discharging mode**

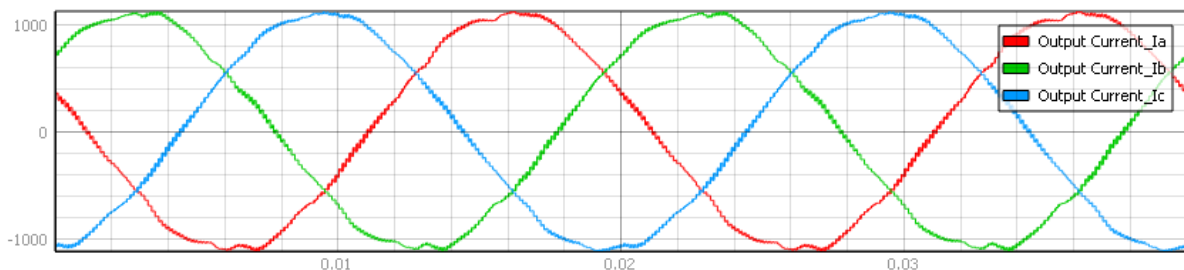


**Figure 64: Output current waveforms in real-time simulation in SC discharging mode**

By PMS command, the SC power converter switches from discharging mode to charging mode when the SoC reaches 40%. SC charges up to 100% to provide the power to the load again. By designing an EMS, the SoC setpoints for switching between charging and discharging modes can be optimized to ensure SC can provides peak demand power. The results for the

moment of switching between discharging and charging mode for SC current at 2000A and 1000A are provided in Figure 65 and Figure 66, respectively. It is shown that the SoC is decreasing to 40%, and then, the power converter reverses the power flow according to the control system, and SoC starts increasing. The output voltage of the DC-DC converter remains constant at the desired value. When SC is in discharging mode the SC current is positive, and it is negative when switches to charging mode. Output current and phase voltage of phase A are also provided in the figures. The output current is in phase with output voltage in discharging mode, meaning that the power is injected from SC to the AC bus. After switching to charging mode, due to the reverse power flow, the output current phase has 180 phase shifts to phase voltage.

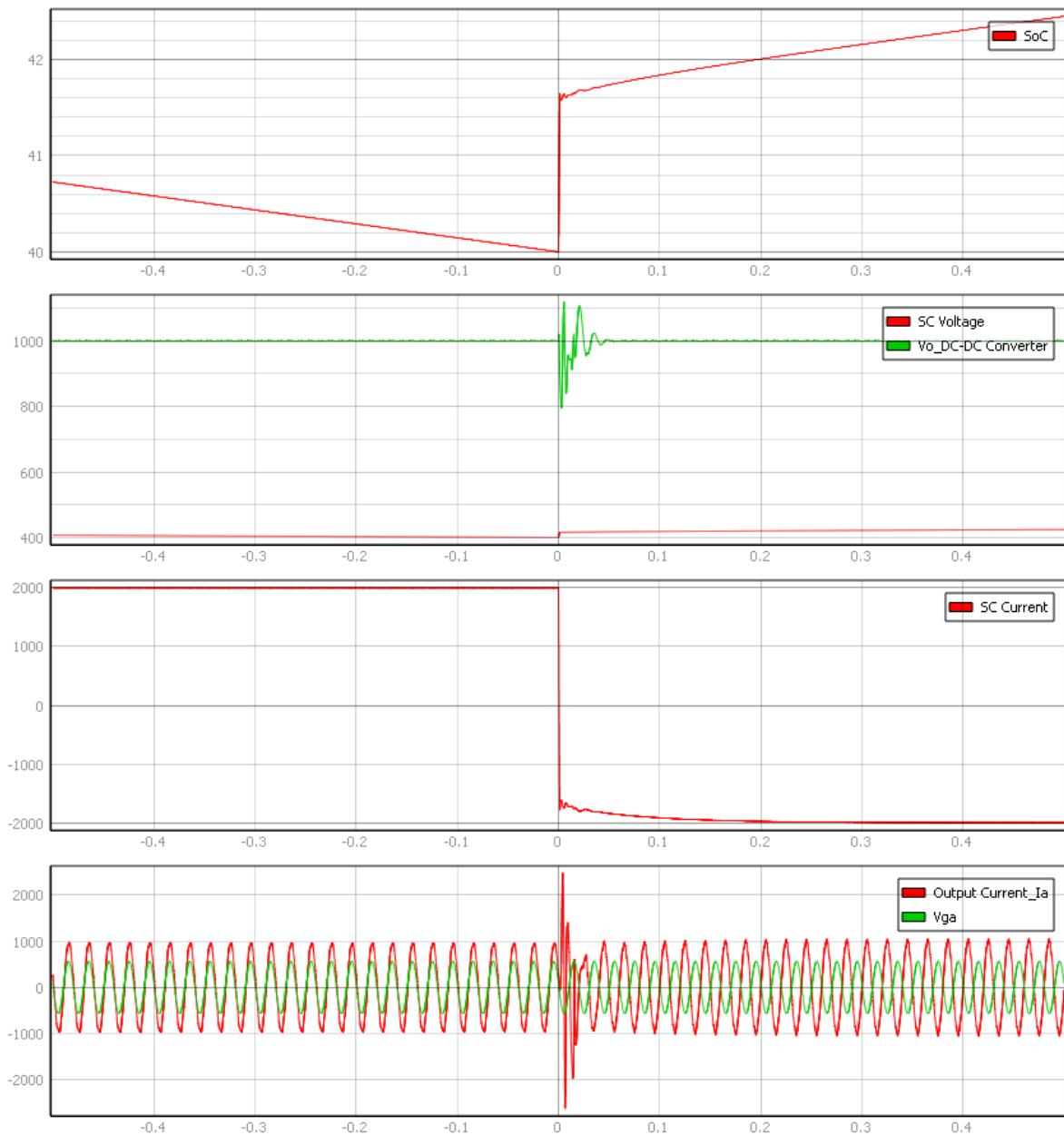


Figure 65: Discharging/charging waveforms of SC at 2000A

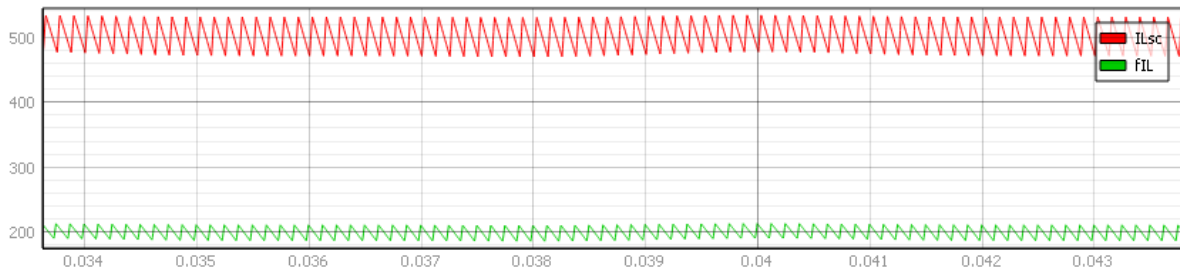


Figure 66: Discharging/charging waveforms of SC at 1000A

### 5.3 Use case 3

The real-time simulation for UC#3 validates the performance of the hybrid ESS (SSB and SC) operation, and they can be a replacement for diesel generators. In this use case, the simulation is done for various setpoints for injected current from both SSB and SC to the load. In the following results, the SSB and SC are both in discharging mode.

First, the SSB reference current is set to 200A (half of its maximum power), and the SC reference current increased from 500A to 2000A. The results are provided in Figure 67, Figure 68, and Figure 69.



**Figure 67: SC and SSB current waveform in ( $I_{ref\_SC} = 500A$ ,  $I_{ref\_SSB} = 200A$ )**

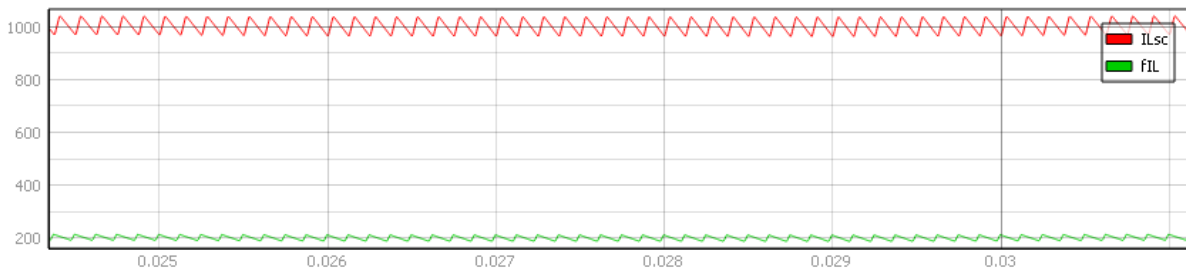


**Figure 68: SC and SSB current waveform ( $I_{ref\_SC} = 1000A$ ,  $I_{ref\_SSB} = 200A$ )**



**Figure 69: SC and SSB current waveform ( $I_{ref\_SC} = 2000A$ ,  $I_{ref\_SSB} = 200A$ )**

Next, the SSB reference current is set to 400A to deliver its maximum power to the load, while the SC reference current is set to 1000A and 2000A, which the waveforms are provided in Figure 70 and Figure 71, respectively. These results show that the SSB can deliver the continuous current to the load, while the SC can quickly provide the peak demand to the load.

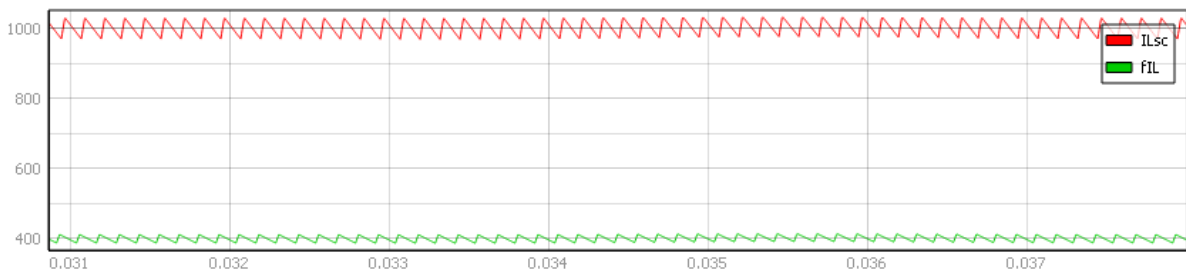


**Figure 70: SC and SSB current waveform ( $I_{ref\_SC} = 1000A$ ,  $I_{ref\_SSB} = 400A$ )**



**Figure 71: SC and SSB current waveform ( $I_{ref\_SC} = 2000A$ ,  $I_{ref\_SSB} = 400A$ )**

## 6 Conclusions and future work

### 6.1 Summary of D5.1

The HIL simulation models developed for ship power system and control system under D5.1 (WP5) are the first step towards the PHIL based testing of the feasibility and validation of the next-generation ESS, namely SSB, SC, and hybrid SSB/SC systems. The models integrating all the elements of the developed ESS architectures have been fine-tuned to match the real data of the use cases and validated with a CHIL setup which will be extended in the next tasks to include the real hardware components. The HIL results demonstrated ESS charging and discharging dynamics at various operating levels, along with steady-state current behaviour, output current waveforms, DC link voltage stability, output power performance, and THD. With the planned PHIL setup, repeatable experimentation of ship power systems becomes feasible, effectively connecting theoretical designs with real-world constraints. The summary of the development work that have been done for this deliverable is as follows:

- **Power and control system design:** This deliverable begins with designing the shipboard microgrid architecture, power converters, required control strategies, and controller design. This step is performed considering original shipboard architectures, integration of novel ESS solutions, and optimization results in previous WPs.
- **Power management system development:** The power management system is to balance the power among power generation units based on their capacity and other requirements, ensuring power stability in the system. According to power generation units' data, the PMS algorithm is specified. The proper power sharing scheme is also discussed, in which the droop control strategy is designed.
- **Integration of developed models into real-time simulator:** The developed microgrids as well as ESS models are implemented in Typhoon HIL environment. Required conversions for modelling is done to integrate data from previous WPs into this deliverable.
- **Implementation of CHIL setup:** The developed control system in this task, is discretized to be implemented in digital signal processing unit. By connecting the real-time simulator and microcontrollers through proper interface, the CHIL setup is established.
- **Performing CHIL simulations:** The real-time simulation is performed for numerous cases and different conditions. A HIL SCADA for every use case is developed to easily monitor the parameters of shipboard power system and ESS. It is also possible to manage the value of parameters and make desired changes in a real-time manner and observe their effects on the performance of the system.
- **Results validation:** Finally, the results are achieved and discussed to validate the developed power and control systems.

### 6.2 Plans for transition to next task

Following the completion of proposed CHIL simulations, the next step is downscaled PHIL testing. In T5.2, a downscaled PHIL test bench will be developed, enabling experimental test on prototyped ESS solutions. By validating the developed framework in D5.1, that is the digital representation of the real hardware units, it is feasible to establish the PHIL setup. Therefore, in T5.2, the ESS including both SSB and SC can be replaced by real ones that are prototyped in WP4 or battery emulators in the laboratory. And instead of real-time models of switching devices, power converter units will be used alongside the ESS modules. A grid/load emulator



will be utilized to represent DG/SG and load. By connecting these units in the hardware level and utilizing real-time simulators for the rest of the system, the PHIL setup will be achieved.

### 6.3 Conclusions

The HIL simulations developed in this work provides a foundation for the integration of ESS with conventional ship power systems in maritime applications. Integrating advanced control systems, this setup has shown that next-generation ESS can handle both normal maritime operations and sudden demands or faults. Next, this work will shift to smaller-scale testing (D5.2 and D5.3) to confirm that real ESS modules behave as expected in various real-world conditions. These scaled-down tests will allow rapid design changes and lower costs while using the same core control and management strategies. Final step of this work is the full-scale ship power system testing (D5.4), creating a logical link between pure simulation and on-board deployment. This plan ensures the project's innovative ESS design, focused on low emissions, high efficiency, and operational safety for cost-effective, reliable, and sustainable maritime electrification solutions.

## 7 References

- [1] C. Cervicato, A. D'Ambra, D. Perna, V. Sangermano, M. Oliveira, and D. P. Esposito, "Operational Profiles and Requirements (D1.1, D1.2)," AENEAS Project, EU Horizon 2023-2026.
- [2] A. Begovic, C. Bischof, F. Sellier, and D. H. Torres, "WP2: Vessel Simulation Models (D2.1, D2.2)," AENEAS Project, EU Horizon 2023-2026.
- [3] R. Tessard and M. Y. Arafat, "WP3: Cell Characterization and Electro-Thermal Modeling (D3.1, D3.2)," AENEAS Project, EU Horizon 2023-2026.
- [4] J. Baake and J. B. Vemula, "Module Sizing, Hardware Design, and Assembly (D4.1, D4.2)," AENEAS Project, EU Horizon 2023-2026.
- [5] R. W. Erickson, D. Maksimović, "Fundamentals of Power Electronics", Kluwer Academic, 2001.
- [6] Katsuhiko Ogata. Modern Control Engineering. 5th ed., Prentice Hall, 2010.
- [7] J. Estaller, A. Kersten, M. Kuder, A. Mashayekh, J. Buberger, T. Thiringer, "Battery impedance modeling and comprehensive comparisons of state-of-the-art cylindrical 18650 battery cells considering cells' price, impedance, specific energy and c-rate," 2021 IEEE International Conference on Environment and Electrical Engineering and 2021 IEEE Industrial and Commercial Power Systems Europe (EEEIC/I&CPS Europe), Sep. 2021, pp. 1-8.
- [8] Battery Cell Model. Typhoon HIL Documentation, Typhoon HIL, 2025. Typhoon HIL.
- [9] T. Dragičević, J. M. Guerrero, J. C. Vasquez and D. Škrlec, "Supervisory Control of an Adaptive-Droop Regulated DC Microgrid With Battery Management Capability," in IEEE Transactions on Power Electronics, vol. 29, no. 2, pp. 695-706, Feb. 2014.
- [10] V. Blasko and V. Kaura, "A new mathematical model and control of a three-phase AC-DC voltage source converter," in IEEE Transactions on Power Electronics, vol. 12, no. 1, pp. 116-123, Jan. 1997.

## 8 Abbreviation list

ESS: Energy Storage Solution

HIL: Hardware-in-the-loop

PHIL: Power Hardware-in-the-loop

CHIL: Controller Hardware-in-the-loop

PMS: Power Management System

SC: Super Capacitor

SSB: Solid State Battery

SoC: State of Charge

BW: Band Width

GM: Gain Margin

PM: Phase Margin

PLL: Phase Locked Loop

VCM: Voltage Controlled Mode

ECM: Equivalent Circuit Model

OCV: Open Circuit Voltage

PWM: Pulse Width Modulation

ADC: Analogue to Digital Converter

THD: Total Harmonic Distortion

## 9 Acknowledgements and disclaimer

The author(s) would like to thank the partners in the project for their valuable contributions on previous drafts.

#	Partner	Partner full name
1	FM	FLANDERS MAKE
2	CEA	COMMISSARIAT A L ENERGIE ATOMIQUE ET AUX ENERGIES ALTERNATIVES
3	ABEE	AVESTA BATTERY & ENERGY ENGINEERING
4	SIE	SIEMENS INDUSTRY SOFTWARE SAS
5	UVA	VAASAN YLIOPISTO
6	I2M	I2M UNTERNEHMENSENTWICKLUNG GMBH
7	GRIM	GRIMALDI EUROMED SPA
8	INLS	INLAND SHIPPING SRL
9	FV	FUNDACION DE LA COMUNIDAD VALENCIANA PARA LA INVESTIGACION, PROMOCION Y ESTUDIOS COMERCIALES DE VALENCIAPORT
10	AUTH	ARISTOTELIO PANEPISTIMIO THESSALONIKIS
11	SOER	FUNDACION CENTRO TECNOLOGICO SOERMAR
12	FMAR	FORMARE- POLO NAZIONALE PER LO SHIPPING SRL
13	ISSN	INSTITUTE FOR SUSTAINABLE SOCIETY AND INNOVATION
14	FS	CONSTRUCCIONES NAVALES P FREIRE SA

### LEGAL DISCLAIMER

Copyright ©, all rights reserved. No part of this report may be used, reproduced and or/disclosed, in any form or by any means without the prior written permission of AENEAS and the AENEAS Consortium. Persons wishing to use the contents of this study (in whole or in part) for purposes other than their personal use are invited to submit a written request to the project coordinator.

The authors of this document have taken any available measure in order for its content to be accurate, consistent and lawful. However, neither the project consortium as a whole nor the individual partners that implicitly or explicitly participated in the creation and publication of this document shall be liable or responsible, in negligence or otherwise, for any loss, damage or expense whatever sustained by any person as a result of the use, in any manner or form, of any knowledge, information or data contained in this document, or due to any inaccuracy, omission or error therein contained.



Funded by  
the European Union

## List of Figures

Figure 1: Block diagram of HIL model development strategy .....	11
Figure 2: Shipboard microgrid for UC#1 (SSB) .....	12
Figure 3: Bidirectional DC-DC converter.....	12
Figure 4: LCL filter with passive damping resistance .....	14
Figure 5: Power generation units for UC#1.....	15
Figure 6: Power management algorithm based on load profile for UC#1 .....	16
Figure 7: Current loop control for DC-DC converter .....	17
Figure 8: Closed loop bode diagram for current loop .....	17
Figure 9: Step response of current loop control system .....	18
Figure 10: Dual loop control of DC-DC converter.....	18
Figure 11: Closed loop bode diagram for dual loop control.....	19
Figure 12: Step response of dual loop control system .....	19
Figure 13: Dual-loop control system with droop strategy .....	19
Figure 14: Dual-loop control for the inverter in grid-following mode .....	20
Figure 15: Bode diagram of open-loop transfer function for the inner-loop.....	21
Figure 16: Bode diagram of the closed-loop system for the inverter dual loop system.....	21
Figure 17: Bode diagram of closed-loop system in VCM .....	22
Figure 18: Step response of the closed-loop system in VCM.....	22
Figure 19: ECM for SSB .....	23
Figure 20: Equivalent thermal model for SSB .....	23
Figure 21: Battery cell model in Typhoon HIL .....	24
Figure 22: Shipboard microgrid for UC#2 (SC) .....	25
Figure 23: Bidirectional DC-DC converter with SC module .....	25
Figure 24: LCL filter with passive damping resistance .....	27
Figure 25: Power generation units for UC#2.....	28
Figure 26: Current loop control for DC-DC converter .....	29
Figure 27: Closed loop bode diagram for current loop .....	29
Figure 28: Step response of current loop control system .....	30
Figure 29: Dual loop control of DC-DC converter.....	30
Figure 30: Closed loop bode diagram for dual loop control.....	31
Figure 31: Step response of dual loop control system .....	31
Figure 32: Dual-loop control for the inverter in grid-following mode .....	32
Figure 33: Bode diagram of open-loop transfer function for the inner-loop.....	32
Figure 34: Bode diagram of the closed-loop system for the inverter dual loop system.....	33
Figure 35: Dynamic SC phenomena modelled with an ECM.....	34
Figure 36: Shipboard microgrid for UC#3 .....	35
Figure 37: Dual loop control of DC-DC converter.....	36
Figure 38: Closed loop bode diagram for dual loop control.....	36
Figure 39: Step response of dual loop control system .....	37
Figure 40: Bode diagram of the closed-loop system for the inverter dual loop system.....	37
Figure 41: CHIL Setup.....	39
Figure 42: Shipboards microgrids and Typhoon HIL device.....	39
Figure 43: Control system and microcontrollers.....	40
Figure 44: Typhoon HIL and microcontrollers interaction.....	40
Figure 45: HIL SCADA for UC#1 .....	41
Figure 46: Steady state DC-link voltage waveform in real-time simulation in mode 3 and mode 7 .....	42
Figure 47: DC-link voltage in transition from mode 7 to mode 3.....	42
Figure 48: Inverter output currents in mode 7 .....	42

Figure 49: Inverter output currents in mode 3 .....42

Figure 50: Inverter output currents in transition between mode 7 and mode 3.....43

Figure 51: Output current of SSB1 and SSB2 at 180A.....43

Figure 52: Steady state output voltage waveform in real-time simulation in mode 2 .....43

Figure 53: Steady state output current waveform in real-time simulation in mode 2.....44

Figure 54: Steady state DC-link voltage waveform in real-time simulation in mode 2 .....44

Figure 55: Steady state SSB current waveforms in real-time simulation in mode 2.....44

Figure 56: Output power and SoC of SSB1 and SSB2 during 6-hour simulation.....45

Figure 57: Output power and SoC of SSB1 and SSB2 during 6-hour simulation.....45

Figure 58: HIL SCADA for UC#2 .....46

Figure 59: Steady state DC-link voltage waveform in real-time simulation in SC charging mode .....46

Figure 60: Steady state SC current waveforms in real-time simulation in SC charging mode .....46

Figure 61: Steady state AC side current waveform in real-time simulation in SC charging mode .....47

Figure 62: DC-link voltage waveform in real-time simulation in SC discharging mode .....47

Figure 63: SC current waveform in real-time simulation in SC discharging mode .....47

Figure 64: Output current waveforms in real-time simulation in SC discharging mode.....47

Figure 65: Discharging/charging waveforms of SC at 2000A .....48

Figure 66: Discharging/charging waveforms of SC at 1000A .....49

Figure 67: SC and SSB current waveform in ( $I_{ref\_SC} = 500A$ ,  $I_{ref\_SSB} = 200A$ ) .....50

Figure 68: SC and SSB current waveform ( $I_{ref\_SC} = 1000A$ ,  $I_{ref\_SSB} = 200A$ ) .....50

Figure 69: SC and SSB current waveform ( $I_{ref\_SC} = 2000A$ ,  $I_{ref\_SSB} = 200A$ ) .....50

Figure 70: SC and SSB current waveform ( $I_{ref\_SC} = 1000A$ ,  $I_{ref\_SSB} = 400A$ ) .....50

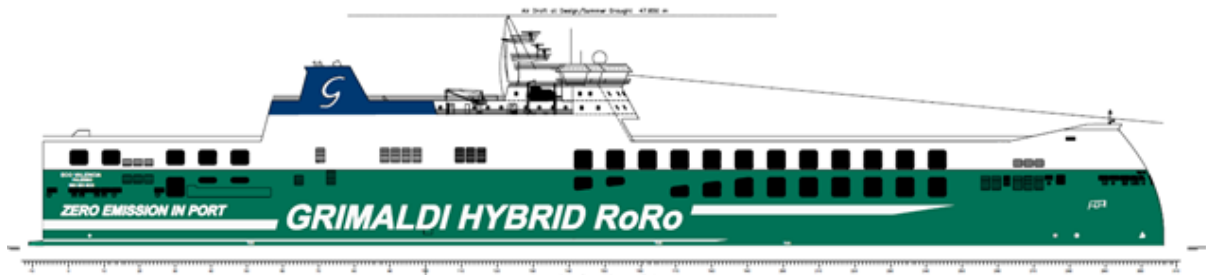
Figure 71: SC and SSB current waveform ( $I_{ref\_SC} = 2000A$ ,  $I_{ref\_SSB} = 400A$ ) .....51



## List of Tables

Table 1: DC-DC converter specifications for UC#1 .....	12
Table 2: DC-AC converter specifications for UC#1 .....	13
Table 3: DC-DC converter specifications for UC#2 .....	26
Table 4: DC-AC converter specifications for UC#2 .....	26
Table 5: Ro-Ro ship technical data sheet .....	60
Table 6: Cruise ship technical data sheet .....	62

## Annex 1: General arrangement and technical specification of Ro-ro ships



Ro-Ro ship general arrangement

Table 5: Ro-Ro ship technical data sheet

<b>Vessel</b>	Ro-Ro ship	
	Type	RO-RO CARGO SHIP
	Flag	Italian
<b>Built</b>	Yard	Jiangsu Jinling Shipyard Company Limited, Yizheng, CHINA
	Delivered	2020 - 2022
<b>Classification</b>	Class assigned	CX, Ro-Ro Cargo Ship, INWATERSURVEY, BWM-T, AUT-UMS, SYS-NEQ-1, SYS-IBS, GREEN PLUS, UNRESTRICTED NAVIGATION
	Class	RINA
<b>Dimensions</b>	Length overall	238.00 m
	Length b.p.	229.75 m
	Moulded breadth	34.00 m
	Depth to main deck, moulded (dk3)	9.30 m
	Depth to wather deck, moulded (dk7)	28.85 m
	Design/smmer max draught (moulded)	7.20 m
	Deadwight ad design draught	18128 t
<b>Tonnage Temporary</b>	GT	67311
	NT	41147
<b>Total number of persons</b>	Passengers/Drivers and crew	12 and 33

<b>Machinery</b>	Main engines	n°2: HYUNDAI-MAN B&W 9S50ME-C9.6- Tier II SMCR = 2 x 12780 kW @ 117 rpm
	Shaft Generators	2 x 2000 kWe
	Bow thrusters	2 x 2000 kWe
	Propeller	2 Controllable Pitch, four (4) blades Dia. 5.8 m
<b>Electric Generator</b>		n°3: Hyundai – HiMSEN 7H21/32 (HR) 3 x 1540 kW @ 1000 rpm run. on HFO&MGO
<b>Hybrid Battery System</b>		2 x 2500 kWh
<b>Air Lubrication System</b>		SILVERSTREAM® TECHNOLOGIES B.V.
<b>Scrubbers (EGCS)</b>		2 x in-line/"hybrid ready"/open loop on ME (ECOSPRAY)
<b>Stern Ramp/door SB</b>	Dimension (LxB)	15 (+3)m x 18m
	Maximum Load	250t SWL
	Maximum axle load	60 t/4wheel
<b>Stern Ramp/door PS</b>	Dimension (LxB)	15 (+3)m x 6m
	Maximum Load	120t SWL
	Maximum axle load	60 t/4wheel
<b>Cargo capacity</b>	Cars	Ab.180
	Gross LM (m)	7800
	Trailers	500

## Annex 2: General arrangement and technical specification of Cruise – series ship

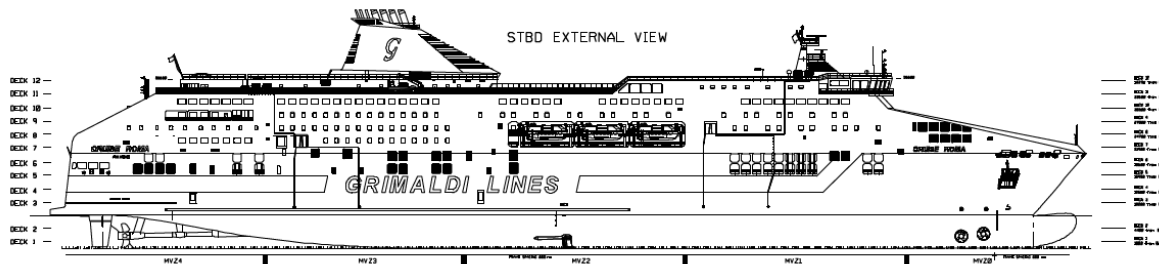


Table 6: Cruise ship technical data sheet

<b>Vessel</b>	Cruise Ship	
	Type	Ro-Ro Passenger ship
	Flag	Italian
<b>Built</b>	Yard	Fincantieri
	Delivered	04/09/2009
	Lengthened	27/06/2019
<b>Classification</b>	Class assigned	C; ro-ro passenger ship; unrestricted navigation; AUT-UMS; MON-SHAFT; AUT-PORT; IWS
	Class	RINA
<b>Dimensions</b>	Length overall	253,80 m
	Length b.p.	231,62 m
	Moulded breadth	30,4 m
	Moulded depth	10,00 m
	Depth to upper deck	21,90 m
	Maximum draft	7,20 m
	Full load displacement	33830,5 t
<b>Tonnage</b>	GT	63742
	NT	35609
	Passengers/Drivers	3343
	Crew	157

<b>Accommodation</b>	Beds	1994
	Cabins	499
		Suites: 18 Superior (4 pers) + 50 Junior (4 pers)
		external: 129 (4 pers)
		internal: 300 (4 pers)
	Handicap: 2 (3 pers)	

<b>Air seats</b>		595 (+302P+5P in conference room)
<b>Trade</b>	Area	Mediterranean Sea – Italy / Spain
	Ports	Civitavecchia – Porto Torres – Barcelona
<b>Machinery</b>	Main engines	4 Wartsila 12v46D
	Power	4X 13860 kW =55440 kW
	Fuel type	IFO 380
	Auxiliary engines	3 Wartsila 8L26A, 3x2550 kW
	Shaft Generators	2x2300 kW
	Hybrid Battery System	2x2735 kWh (CORVUS)
	Scrubbers (EGCS)	4xOpen Loop type on ME (ECOSPRAY)
	Bowthrusters	2x1850 kW
	Sternthrusters	-
	Propeller	2 Wartsila
	Stabilizer	2 Fincantieri
<b>Electric system</b>	Main power	690/230 V 50Hz
	Emergency power batteries	24 V
<b>Tank capacities</b>	Fuel oil	1700,0 m3
	Diesel Oil	485,0 m3
	Fresh Water	1422 m3
	Ballast water	3411,0 m3
<b>Ramps</b>	External ramps	2 stern ramps
	Dimensions (LxB)	10 (+2.5) x 11.5 m
<b>Cargo capacity</b>		60 t
	Cars	266
	L/mt	3720
	Trailers (15m)	233